Accounting for scalar non-Gaussianity in secondary gravitational waves

H. V. Ragavendra[*]

Centre for Strings, Gravitation and Cosmology, Department of Physics,
Indian Institute of Technology Madras, Chennai 600036, India

It is well known that enhancement in the primordial scalar perturbations over small scales generates detectable amplitudes of secondary gravitational waves (GWs), by sourcing the tensor perturbations at the second order. These stochastic gravitational waves are expected to carry the imprints of primordial non-Gaussianities. The scalar bispectrum that is typically produced in models of inflation leading to significant secondary GWs is non-trivial and highly scale-dependent. In this work, we present a method to account for such general scale-dependent scalar bispectrum arising from inflationary models in the calculation of the spectral density of secondary GWs. Using this method, we compute the contributions arising from the scalar bispectrum to the amplitude of secondary GWs in two specific models of inflation driven by the canonical scalar field. We find that these non-Gaussian contributions can be highly model dependent and have to be consistently taken into account while estimating the total amplitude of the secondary GWs. Beyond the models considered, we emphasize that the method discussed is robust, free from assumptions about the shape of the bispectrum and generalizes earlier approaches adopted in the literature. We argue that this method of accounting for the scalar bispectrum shall be helpful in future computations for exotic models generating larger amplitudes of scalar non-Gaussianities along with significant amount of secondary GWs.

I. INTRODUCTION

Models of inflation leading to enhanced scalar power over small scales are examined in the context of production of primordial black holes (PBHs) and the associated secondary gravitational waves (GWs). In these models, modes of scalar perturbations that have amplitudes large enough to form PBHs, also enhance the tensor perturbations by sourcing them at the second order. This leads to generation of secondary GWs of strengths detectable in the present universe (see, for instance, Refs. [1–6] for discussions and constraints). Typical inflationary models considered in this context that are driven by a canonical scalar field, permit a brief epoch of ultra slow roll amidst an otherwise slow roll evolution of the inflaton field (see, for instance, Refs. [7–11]). This epoch is known to enhance the amplitude of curvature perturbations and lead to large amplitudes of scalar power over small scales. The production of PBHs is exponentially sensitive to the amplitude of scalar power and hence highly dependent on the behavior of the spectrum around the small range of wavenumbers close to the peak. However, the spectrum of secondary GWs is proportional to the square of the scalar power spectrum sourcing it. Therefore, it can better capture any feature that may be present in the scalar power spectrum over a wider range of wavenumbers.

Besides, there have been efforts to quantify the effect of the primordial scalar non-Gaussianity on the predicted signals of secondary GWs [12–17]. The general approach is to account for corrections in the power spectrum arising due to the scalar bispectrum through the non-Gaussianity parameter f_{NL}. There are usually well-motivated assumptions made about the shape of f_{NL} being local in such calculations. However, in realistic models of inflation, we find that, though f_{NL} is local close to the peak of the scalar power spectrum, it is highly scale dependent over a wide range of wavenumbers. Moreover, it has been shown that the consistency condition relating the power spectrum and the bispectrum in the squeezed limit is satisfied in canonical single field models considered in these scenarios [11, 18]. Therefore, it is important to take into account the complete form of the bispectrum in calculating the correction to the power spectrum and examining the imprints of scalar non-Gaussianity on the secondary GWs.

In this work, we present a method to account for a general, scale-dependent f_{NL}, in such a calculation, by reconsidering the definition of the parameter. This method does not assume any shape or template for f_{NL} or the scalar bispectrum. Nevertheless it is consistent with the previous approaches when the assumptions are invoked, *i.e.* it reduces to earlier methods adopted if the f_{NL} is assumed to be of a certain shape, say, a local form. This allows us to capture the complete behavior of the bispectrum along with any non-trivial features that may be present therein and examine its imprint on the spectrum of GWs generated. We illustrate this method of accounting for scalar bispectrum using two models as examples. One is a toy model of inflation constructed by adding an artificial dip to the otherwise smooth potential permitting slow roll evolution of the field [19, 20]. The second is a model of inflation known as

---

critical-Higgs inflation which is motivated by Higgs field driving inflation while containing an inflection point in the potential [21–23]. Both these models serve as interesting examples for a typical scenario of inflation where the field undergoes an interim epoch of ultra slow roll during its evolution. We calculate the scalar bispectrum in these models and compute the corresponding correction to the power spectrum. We further compute the non-Gaussian contributions to the dimensionless spectral energy density of secondary GWs, $i.e.$ Ω_{GW}, generated in these models.

The structure of the paper is as follows. In the next section, we present the generalized definition of the non-Gaussianity parameter f_{NL} to include a generic scale dependence. We also outline the steps involved in calculating f_{NL} from the cubic order action of the scalar perturbations. We then arrive at the expression for the correction to be added to the scalar power spectrum, $viz.$ $\mathcal{P}_{\mathrm{C}}(k)$ in section III. In section IV, we shall compute the non-Gaussian contributions to Ω_{GW} arising due to f_{NL}. We shall point out that some of these contributions can be expressed in terms of $\mathcal{P}_{\mathrm{C}}(k)$. We present the models for illustration in section V, and compute the power and bi-spectra arising from them. We shall calculate the corrections to the power spectra using the respective bispectra and compare against the original spectra. We also obtain an analytical estimate of the correction and compare it against the exact numerical result. We shall finally evaluate the Ω_{GW} generated from these models due to both Gaussian and non-Gaussian contributions and compare the amplitudes in each case. We conclude in section VI with a brief summary and outlook.

Before proceeding, let us clarify the notations that shall be used in this work. We work with natural units such that $\hbar = c = 1$ and set the reduced Planck mass to be $M_{\mathrm{Pl}} = (8\,\pi\,G)^{-1/2}$. We shall assume the background to be the spatially flat Friedmann-Lemaître-Robertson-Walker (FLRW) line element described by the scale factor a and the Hubble parameter H. The Greek letter η shall represent the conformal time coordinate.

II. SCALE DEPENDENT $f_{\mathrm{NL}}(k_1, k_2, k_3)$

In this section, we shall consider the conventional definition of the scalar non-Gaussianity parameter f_{NL} and generalize it to account for a generic scale dependence. The parameter f_{NL} is conventionally defined using the relation [24, 25]

$$\mathcal{R}(\boldsymbol{x}, \eta) = \mathcal{R}^{\mathrm{G}}(\boldsymbol{x}, \eta) - \frac{3}{5} f_{\mathrm{NL}} [\mathcal{R}^{\mathrm{G}}(\boldsymbol{x}, \eta)]^2 \,, \tag{1}$$

where $\mathcal{R}(\boldsymbol{x}, \eta)$ is the curvature perturbation and $\mathcal{R}^{\mathrm{G}}(\boldsymbol{x}, \eta)$ is the Gaussian part of $\mathcal{R}(\boldsymbol{x}, \eta)$. Evidently, this definition assumes f_{NL} to be local, $i.e.$ independent of wavenumbers. Nevertheless, this is often taken as the definition to calculate the bispectrum even in cases with non-trivial scale dependence. Here, we shall generalize this definition to explicitly account for the scale dependence in the parameter. For this, we consider the above relation in Fourier space and redefine f_{NL} as a function in Fourier space with wavenumbers as its arguments (for similar efforts in different contexts, see, Refs. [26, 27]). We can write such a relation as

$$\mathcal{R}_{\boldsymbol{k}}(\eta) = \mathcal{R}_{\boldsymbol{k}}^{\mathrm{G}}(\eta) - \frac{3}{5} \int \frac{\mathrm{d}^3 \boldsymbol{k_1}}{(2\,\pi)^{3/2}} \mathcal{R}_{\boldsymbol{k_1}}^{\mathrm{G}}(\eta) \mathcal{R}_{\boldsymbol{k}-\boldsymbol{k_1}}^{\mathrm{G}}(\eta) \, f_{\mathrm{NL}}[\boldsymbol{k}, (\boldsymbol{k_1} - \boldsymbol{k}), -\boldsymbol{k_1}] \,, \tag{2}$$

where $\mathcal{R}_{\boldsymbol{k}}$ is the mode function corresponding to the curvature perturbation $\mathcal{R}$, and $\mathcal{R}_{\boldsymbol{k}}^{\mathrm{G}}$ denotes the Gaussian part of $\mathcal{R}_{\boldsymbol{k}}$. We should mention that the $f_{\mathrm{NL}}(k_1, k_2, k_3)$ defined depends only on the magnitude of the three wavevectors in the argument. We have written the arguments in the integrand above as vectors just to emphasize that by construction they form a triangular configuration in the space of wavenumbers ($i.e.$ sum of the three vectors vanishes identically), as is expected of the arguments of the bispectrum. We can also obtain the counterpart of this parameter in real space by looking at the inverse Fourier transform of the above relation

$$\mathcal{R}(\boldsymbol{x}, \eta) = \mathcal{R}^{\mathrm{G}}(\boldsymbol{x}, \eta) - \frac{3}{5} \int \frac{\mathrm{d}^3 \boldsymbol{k}}{(2\pi)^3} \int \mathrm{d}^3 \boldsymbol{k_1} \mathcal{R}_{\boldsymbol{k_1}}^{\mathrm{G}}(\eta) \mathcal{R}_{\boldsymbol{k}-\boldsymbol{k_1}}^{\mathrm{G}}(\eta) \, f_{\mathrm{NL}}[\boldsymbol{k}, (\boldsymbol{k_1} - \boldsymbol{k}), -\boldsymbol{k_1}] \, \mathrm{e}^{i\boldsymbol{k}\cdot\boldsymbol{x}} \,. \tag{3}$$

We should note that this equation reduces to the conventional definition of f_{NL} given in Eq. (1), if $f_{\mathrm{NL}}(k_1, k_2, k_3)$ turns out to be scale independent in a given model. Hence our generalization is consistent with the existing approach to quantify the scalar non-Gaussianity.

A. Relation to the bispectrum

We proceed to establish the relation between the $f_{\mathrm{NL}}(k_1, k_2, k_3)$ given above and the scalar bispectrum, denoted as $G(k_1, k_2, k_3)$. Note that the scalar power spectrum $\mathcal{P}_{\mathrm{S}}(k)$ and the bispectrum $G(k_1, k_2, k_3)$ are defined as

$$\langle \hat{\mathcal{R}}_{\boldsymbol{k_1}} \hat{\mathcal{R}}_{\boldsymbol{k_2}} \rangle = \frac{2\pi^2}{k^3} \mathcal{P}_{\mathrm{S}}(k_1) \, \delta^{(3)}(\boldsymbol{k_1} + \boldsymbol{k_2}) \,, \tag{4a}$$

$$\langle \hat{\mathcal{R}}_{\boldsymbol{k_1}} \hat{\mathcal{R}}_{\boldsymbol{k_2}} \hat{\mathcal{R}}_{\boldsymbol{k_3}} \rangle = (2\pi)^{-3/2} \, G(k_1, k_2, k_3) \, \delta^{(3)}(\boldsymbol{k}_1 + \boldsymbol{k}_2 + \boldsymbol{k}_3) \,, \tag{4b}$$

where $\hat{\mathcal{R}}_{\boldsymbol{k}}$ is an operator obtained by quantizing the mode function $\mathcal{R}_{\boldsymbol{k}}$. To express $f_{\mathrm{NL}}(k_1, k_2, k_3)$ in terms of $G(k_1, k_2, k_3)$ and $\mathcal{P}_{\mathrm{S}}(k)$, we compute the expectation value of the three point correlation of $\hat{\mathcal{R}}_k$. Using the relation given in Eq. (2), we obtain that

$$\langle \hat{\mathcal{R}}_{\boldsymbol{k_1}} \hat{\mathcal{R}}_{\boldsymbol{k_2}} \hat{\mathcal{R}}_{\boldsymbol{k_3}} \rangle = -\frac{3}{5} \int \frac{\mathrm{d}^3 \boldsymbol{k}_1'}{(2\,\pi)^{3/2}} \, \langle \hat{\mathcal{R}}_{\boldsymbol{k_1}}^{\mathrm{G}} \hat{\mathcal{R}}_{\boldsymbol{k_2}}^{\mathrm{G}} \hat{\mathcal{R}}_{\boldsymbol{k_3'}}^{\mathrm{G}} \hat{\mathcal{R}}_{\boldsymbol{k_3} - \boldsymbol{k_3'}}^{\mathrm{G}} \rangle$$
$$\times f_{\mathrm{NL}}[\boldsymbol{k}_3, (\boldsymbol{k}_3' - \boldsymbol{k}_3), -\boldsymbol{k}_3'] + \text{ two permutations.} \tag{5}$$

We should mention that the expectation values are evaluated in a specific initial state, which is assumed to be the Bunch-Davies vacuum. Also, note that the term in the right hand side of the above expression is the leading order term in the expansion assuming $\mathcal{R}^{\mathrm{G}}$ is perturbative. Using Wick's theorem, we can express the four point function in the above integral in terms of the $\mathcal{P}_{\mathrm{S}}(k)$ and simplify it to obtain

$$\langle \hat{\mathcal{R}}_{\boldsymbol{k_1}} \hat{\mathcal{R}}_{\boldsymbol{k_2}} \hat{\mathcal{R}}_{\boldsymbol{k_3}} \rangle = -\frac{3}{5} \frac{4\pi^4}{(2\pi)^{3/2}} \frac{\mathcal{P}_{\mathrm{S}}(k_1)}{k_1^3} \frac{\mathcal{P}_{\mathrm{S}}(k_2)}{k_2^3} \, \delta^{(3)}(\boldsymbol{k}_1 + \boldsymbol{k}_2 + \boldsymbol{k}_3)$$
$$\times \left[f_{\mathrm{NL}}(\boldsymbol{k}_3, \boldsymbol{k}_2, \boldsymbol{k}_1) + f_{\mathrm{NL}}(\boldsymbol{k}_3, \boldsymbol{k}_1, \boldsymbol{k}_2) \right] + \text{ two permutations.} \tag{6}$$

We again emphasize that the arguments of f_{NL} above are given as wavevectors to remind that they satisfy the triangularity condition $\boldsymbol{k}_1 + \boldsymbol{k}_2 + \boldsymbol{k}_3 = \boldsymbol{0}$. We then use the property of the bispectrum being symmetric in its arguments [*i.e.* $G(k_1, k_2, k_3) = G(k_1, k_3, k_2)$], to relate the $f_{\mathrm{NL}}(k_1, k_2, k_3)$ constructed to the power and bi-spectra. We hence obtain the relation

$$f_{\mathrm{NL}}(k_1, k_2, k_3) = -\frac{10}{3} \frac{(k_1 k_2 k_3)^3}{16\pi^4} G(k_1, k_2, k_3) \left[k_1^3 \mathcal{P}_{\mathrm{S}}(k_2) \mathcal{P}_{\mathrm{S}}(k_3) + \text{two permutations} \right]^{-1} \,. \tag{7}$$

This turns out to be the conventional relation used in the literature to compute f_{NL} in terms of $\mathcal{P}_{\mathrm{S}}(k)$ and $G(k_1, k_2, k_3)$ [25, 28–30]. Thus we infer that the $f_{\mathrm{NL}}(k_1, k_2, k_3)$ defined in Eq. (2) is compatible with the conventional relation. The difference in this derivation is that we have explicitly accounted for the scale dependence of the bispectrum in the non-Gaussianity parameter $f_{\mathrm{NL}}(k_1, k_2, k_3)$.

B. Calculation of $G(k_1, k_2, k_3)$ from the cubic order action

Before we proceed to compute the correction to the power spectrum and the non-Gaussian contributions to Ω_{GW} due to $f_{\mathrm{NL}}(k_1, k_2, k_3)$ discussed above, we shall briefly comment on the calculation of the scalar bispectrum $G(k_1, k_2, k_3)$ in a given inflationary model. The quantity $G(k_1, k_2, k_3)$, as defined in Eq. (4b), is evaluated in the perturbative vacuum, at the end of inflation. The bispectrum receives contributions from the third order action governing the curvature perturbation [24, 31–33]. This action, in the case of a canonical scalar field driven inflation, has six terms bulk terms apart from boundary terms. Hence there arises six contributions to the bispectrum due to all the bulk terms. There is also a seventh contribution, arising due to a non-vanishing temporal boundary term, that is typically absorbed using a field redefinition [34]. The explicit forms of these contributions are as follows [25, 28, 30]:

$$G(\boldsymbol{k}_1, \boldsymbol{k}_2, \boldsymbol{k}_3) = \sum_{C=1}^{7} G_C(\boldsymbol{k}_1, \boldsymbol{k}_2, \boldsymbol{k}_3)$$
$$= M_{\mathrm{Pl}}^2 \sum_{C=1}^{6} \left[f_{k_1}(\eta_{\mathrm{e}}) \, f_{k_2}(\eta_{\mathrm{e}}) \, f_{k_3}(\eta_{\mathrm{e}}) \, \mathcal{G}_C(\boldsymbol{k}_1, \boldsymbol{k}_2, \boldsymbol{k}_3) + \text{complex conjugate} \right] + G_7(\boldsymbol{k}_1, \boldsymbol{k}_2, \boldsymbol{k}_3) \,. \tag{8}$$

The terms denoted by $\mathcal{G}_C$ in this expression involve integrals arising from the bulk terms of the third order action. The seventh term G_7 is due to the non-vanishing boundary term mentioned above. The explicit forms of these terms are

$$\mathcal{G}_1(\boldsymbol{k}_1, \boldsymbol{k}_2, \boldsymbol{k}_3) = 2\,i \int_{\eta_{\mathrm{i}}}^{\eta_{\mathrm{e}}} \mathrm{d}\eta \, a^2 \, \epsilon_1^2 \, \left(f_{k_1}^* \, f_{k_2}'^* \, f_{k_3}'^* + \text{two permutations} \right) , \tag{9a}$$

$$\mathcal{G}_2(\boldsymbol{k}_1, \boldsymbol{k}_2, \boldsymbol{k}_3) = -2\,i \, (\boldsymbol{k}_1 \cdot \boldsymbol{k}_2 + \text{two permutations}) \int_{\eta_{\mathrm{i}}}^{\eta_{\mathrm{e}}} \mathrm{d}\eta \, a^2 \, \epsilon_1^2 \, f_{k_1}^* \, f_{k_2}^* \, f_{k_3}^* , \tag{9b}$$

$$\mathcal{G}_3(\boldsymbol{k}_1, \boldsymbol{k}_2, \boldsymbol{k}_3) = -2\,i \int_{\eta_{\mathrm{i}}}^{\eta_{\mathrm{e}}} \mathrm{d}\eta \, a^2 \, \epsilon_1^2 \, \left(\frac{\boldsymbol{k}_1 \cdot \boldsymbol{k}_2}{k_2^2} \, f_{k_1}^* \, f_{k_2}'^* \, f_{k_3}'^* + \text{five permutations} \right) , \tag{9c}$$

$$\mathcal{G}_4(\boldsymbol{k}_1, \boldsymbol{k}_2, \boldsymbol{k}_3) = i \int_{\eta_{\mathrm{i}}}^{\eta_{\mathrm{e}}} \mathrm{d}\eta\, a^2\, \epsilon_1\, \epsilon_2'\, \left(f_{k_1}^*\, f_{k_2}^*\, f_{k_3}'^* + \text{two permutations}\right), \tag{9d}$$

$$\mathcal{G}_5(\boldsymbol{k}_1, \boldsymbol{k}_2, \boldsymbol{k}_3) = \frac{i}{2} \int_{\eta_{\mathrm{i}}}^{\eta_{\mathrm{e}}} \mathrm{d}\eta\, a^2\, \epsilon_1^3\, \left(\frac{\boldsymbol{k}_1 \cdot \boldsymbol{k}_2}{k_2^2}\, f_{k_1}^*\, f_{k_2}'^*\, f_{k_3}'^* + \text{five permutations}\right), \tag{9e}$$

$$\mathcal{G}_6(\boldsymbol{k}_1, \boldsymbol{k}_2, \boldsymbol{k}_3) = \frac{i}{2} \int_{\eta_{\mathrm{i}}}^{\eta_{\mathrm{e}}} \mathrm{d}\eta\, a^2\, \epsilon_1^3\, \left(\frac{k_1^2\, (\boldsymbol{k}_2 \cdot \boldsymbol{k}_3)}{k_2^2\, k_3^2}\, f_{k_1}^*\, f_{k_2}'^*\, f_{k_3}'^* + \text{two permutations}\right), \tag{9f}$$

$$G_7(\boldsymbol{k}_1, \boldsymbol{k}_2, \boldsymbol{k}_3) = -i\, M_{\mathrm{Pl}}^2\, \left[f_{k_1}(\eta_{\mathrm{e}})\, f_{k_2}(\eta_{\mathrm{e}})\, f_{k_3}(\eta_{\mathrm{e}})\right]$$
$$\times \left[a^2\epsilon_1\epsilon_2\, f_{k_1}^*(\eta)\, f_{k_2}^*(\eta)\, f_{k_3}'^*(\eta) + \text{two permutations}\right]_{\eta_i}^{\eta_e} + \text{ complex conjugate}, \tag{9g}$$

where in all these equations, $f_k(\eta)$ denotes the mode function satisfying the Bunch-Davies initial condition and $f_k'(\eta)$ is the derivative of $f_k(\eta)$ with respect to the conformal time η. The quantities ϵ_1 and ϵ_2 are the first and second slow roll parameters that capture the background evolution in a given model of inflation. Moreover, the time η_{i} denotes the conformal time when the initial conditions are imposed on the modes, while η_{e} denotes the conformal time close to the end of inflation.

Using these expressions for the various contributions to the scalar bispectrum, we can evaluate the complete bispectrum $G(k_1, k_2, k_3)$. Upon evaluating the bispectrum, we can readily obtain the non-Gaussianity parameter $f_{\mathrm{NL}}(k_1, k_2, k_3)$ through the relation given in Eq. (7).

III. CORRECTION TO THE POWER SPECTRUM

Having setup a method to account for a generic scale dependence in the non-Gaussianity parameter $f_{\mathrm{NL}}(k_1, k_2, k_3)$, we shall now proceed to compute the non-Gaussian correction to the $\mathcal{P}_{\mathrm{S}}(k)$ arising due to the bispectrum. To compute the correction, which we shall call as $\mathcal{P}_{\mathrm{C}}(k)$, we calculate the two point correlation of $\hat{\mathcal{R}}_k$, using the relation given in Eq. (2) as

$$\langle \hat{\mathcal{R}}_{\boldsymbol{k}_1} \hat{\mathcal{R}}_{\boldsymbol{k}_2} \rangle = \langle \hat{\mathcal{R}}_{\boldsymbol{k}_1}^{\mathrm{G}} \hat{\mathcal{R}}_{\boldsymbol{k}_2}^{\mathrm{G}} \rangle + \frac{9}{25} \int \frac{\mathrm{d}^3 \boldsymbol{k}_1'}{(2\,\pi)^3} \int \mathrm{d}^3 \boldsymbol{k}_2' \langle \hat{\mathcal{R}}_{\boldsymbol{k}_1'}^{\mathrm{G}} \hat{\mathcal{R}}_{\boldsymbol{k}_1 - \boldsymbol{k}_1'}^{\mathrm{G}} \hat{\mathcal{R}}_{\boldsymbol{k}_2'}^{\mathrm{G}} \hat{\mathcal{R}}_{\boldsymbol{k}_2 - \boldsymbol{k}_2'}^{\mathrm{G}} \rangle$$
$$\times f_{\mathrm{NL}}\big(k_1, |\boldsymbol{k}_1' - \boldsymbol{k}_1|, k_1'\big)\, f_{\mathrm{NL}}\big(k_2, |\boldsymbol{k}_2' - \boldsymbol{k}_2|, k_2'\big). \tag{10}$$

On substituting the definition of power spectrum [cf. Eq. (4a)] and expressing the four point correlation in terms of the two point correlations as before, the above equation leads to

$$\mathcal{P}_{\mathrm{S}}^{\mathrm{M}}(k) = \mathcal{P}_{\mathrm{S}}(k) + \frac{9}{50\pi} k^3 \int \mathrm{d}^3 \boldsymbol{k}_1\, \frac{\mathcal{P}_{\mathrm{S}}(k_1)}{k_1^3} \frac{\mathcal{P}_{\mathrm{S}}(|\boldsymbol{k} - \boldsymbol{k}_1|)}{|\boldsymbol{k} - \boldsymbol{k}_1|^3}\, f_{\mathrm{NL}}^2[k, |\boldsymbol{k}_1 - \boldsymbol{k}|, k_1], \tag{11}$$

where $\mathcal{P}_{\mathrm{S}}(k)$ denotes the original power spectrum corresponding to the Gaussian perturbations $\mathcal{R}^{\mathrm{G}}$ and $\mathcal{P}_{\mathrm{S}}^{\mathrm{M}}(k)$ denotes the spectrum with the non-Gaussian correction taken into account. Therefore, we can identify the correction $\mathcal{P}_{\mathrm{C}}(k)$, that is to be added to the original spectrum $\mathcal{P}_{\mathrm{S}}(k)$, as

$$\mathcal{P}_{\mathrm{C}}(k) = \frac{9}{50\pi} k^3 \int \mathrm{d}^3 \boldsymbol{k}_1\, \frac{\mathcal{P}_{\mathrm{S}}(k_1)}{k_1^3} \frac{\mathcal{P}_{\mathrm{S}}(|\boldsymbol{k} - \boldsymbol{k}_1|)}{|\boldsymbol{k} - \boldsymbol{k}_1|^3}\, f_{\mathrm{NL}}^2[k, |\boldsymbol{k}_1 - \boldsymbol{k}|, k_1]. \tag{12}$$

We should note that there can be additional terms to this correction which involve the irreducible part of the four point correlation, viz. the trispectrum of scalar perturbations [13, 14, 17]. Such terms shall receive contributions from higher order terms of the action and hence will be at higher order in perturbations than the terms we are working with. We believe those terms are beyond the scope of this work. In our analysis we shall restrict ourselves to the terms of four point correlations reduced in terms of the power spectra.

To simplify the above expression for $\mathcal{P}_{\mathrm{C}}(k)$ we perform a suitable change of variables. Defining a variable $u = |\boldsymbol{k} - \boldsymbol{k}_1|$, we get

$$\mathcal{P}_{\mathrm{C}}(k) = \frac{9}{25} k^2 \int_0^\infty \frac{\mathrm{d}k_1}{k_1^2}\, \mathcal{P}_{\mathrm{S}}(k_1) \int_{|\boldsymbol{k} - \boldsymbol{k}_1|}^{|\boldsymbol{k} + \boldsymbol{k}_1|} \frac{\mathrm{d}u}{u^2}\, \mathcal{P}_{\mathrm{S}}(u)\, f_{\mathrm{NL}}^2[k, u, k_1]. \tag{13}$$

Further introducing $x = k_1/k$ and $y = u/k$, we get,

$$\mathcal{P}_{\mathrm{C}}(k) = \frac{9}{25} \int_0^\infty \mathrm{d}x \int_{|1-x|}^{|1+x|} \mathrm{d}y\, \frac{\mathcal{P}_{\mathrm{S}}(kx)}{x^2} \frac{\mathcal{P}_{\mathrm{S}}(ky)}{y^2}\, f_{\mathrm{NL}}^2[k, kx, ky]. \tag{14}$$

Again, we can notice that if $f_{\mathrm{NL}}(k_1, k_2, k_3)$ turns out to be scale independent we recover the expression for $\mathcal{P}_{\mathrm{C}}(k)$ that is used in case of a local f_{NL} [12–15]. If we use the relation between $f_{\mathrm{NL}}(k_1, k_2, k_3)$ and the power and bi-spectra [cf. Eq. (7)], we can write down $\mathcal{P}_{\mathrm{C}}(k)$ explicitly in terms of $G(k_1, k_2, k_3)$ and $\mathcal{P}_{\mathrm{S}}(k)$ as

$$
\mathcal{P}_{\mathrm{C}}(k) = \frac{4\,k^{12}}{(2\pi)^8} \int_0^\infty \mathrm{d}x \int_{|1-x|}^{1+x} \mathrm{d}y \, \frac{x^4 y^4}{\mathcal{P}_{\mathrm{S}}(kx)\,\mathcal{P}_{\mathrm{S}}(ky)} \, G^2(k, kx, ky) \left[1 + x^3 \frac{\mathcal{P}_{\mathrm{S}}(k)}{\mathcal{P}_{\mathrm{S}}(kx)} + y^3 \frac{\mathcal{P}_{\mathrm{S}}(k)}{\mathcal{P}_{\mathrm{S}}(ky)} \right]^{-2}. \tag{15}
$$

We should mention here that, because of the well regulated nature of the integral involved, we shall use Eq. (14) as the working definition for computing $\mathcal{P}_{\mathrm{C}}(k)$.

IV. COMPUTATION OF Ω_{GW} ACCOUNTING FOR f_{NL}

Having obtained the correction to the power spectra, $\mathcal{P}_{\mathrm{C}}(k)$, we shall proceed to compute the non-Gaussian contributions to Ω_{GW}. During the computation of Ω_{GW} there may arise contributions from f_{NL} other than from $\mathcal{P}_{\mathrm{C}}(k)$. These are referred to as connected contributions in the literature [12, 13, 17]. We should note that there are arguments in the literature suggesting that these contributions vanish identically when integrated over azimuthal angles involved in the corresponding integrals [12, 14]. However, detailed calculations suggest that this may not be the case when accounted for exact dependence of the integrand over these angles appropriately [17]. In this work, we shall compute all the terms involved while consistently accounting for a scale dependent f_{NL} in them. We shall later compare the respective contributions against the contribution from the original power spectrum to the estimate of Ω_{GW}, when we consider specific models for illustration.

To begin with, let us recall the calculation of the secondary tensor power spectrum in terms of the scalar power spectrum (for some of the earlier discussions, see Refs. [1, 2]; for some of the recent efforts, see, Refs. [4, 5, 11, 35–38]). The two point correlation of the secondary tensor perturbation $h_k^\lambda(\eta)$ is related to the scalar perturbation $\mathcal{R}_{\boldsymbol{k}}$ as

$$
\begin{aligned}
\langle \hat{h}_{\boldsymbol{k}_1}^\lambda(\eta)\, \hat{h}_{\boldsymbol{k}_2}^{\lambda'}(\eta) \rangle = {}& \frac{16}{81} \frac{1}{k_1 k_2 \eta^2} \int \frac{\mathrm{d}^3 \boldsymbol{p}}{(2\pi)^{3/2}} \int \frac{\mathrm{d}^3 \boldsymbol{p}'}{(2\pi)^{3/2}} \, Q^\lambda(k_1, p)\, Q^{\lambda'}(k_2, p') \\
& \times \left[\mathcal{I}_c\left(\frac{p}{k_1}, \frac{|\boldsymbol{k}_1 - \boldsymbol{p}|}{k_1} \right) \cos(k_1\,\eta) + \mathcal{I}_s\left(\frac{p}{k_1}, \frac{|\boldsymbol{k}_1 - \boldsymbol{p}|}{k_1} \right) \sin(k_1\,\eta) \right] \\
& \times \left[\mathcal{I}_c\left(\frac{p'}{k_2}, \frac{|\boldsymbol{k}_2 - \boldsymbol{p}'|}{k_2} \right) \cos(k_2\,\eta) + \mathcal{I}_s\left(\frac{p'}{k_2}, \frac{|\boldsymbol{k}_2 - \boldsymbol{p}'|}{k_2} \right) \sin(k_2\,\eta) \right] \\
& \times \langle \hat{\mathcal{R}}_{\boldsymbol{p}}\, \hat{\mathcal{R}}_{\boldsymbol{k}_1 - \boldsymbol{p}}\, \hat{\mathcal{R}}_{\boldsymbol{p}'}\, \hat{\mathcal{R}}_{\boldsymbol{k}_2 - \boldsymbol{p}'} \rangle,
\end{aligned} \tag{16}
$$

where the functions $\mathcal{I}_{c,s}(u, v)$ arise due to the transfer function relating the Bardeen potential during the radiation dominated epoch to the primordial curvature perturbation. The form of these functions are described as

$$
\mathcal{I}_c(v, u) = -\frac{27\,\pi}{4\,v^3\,u^3}\, \Theta\left(v + u - \sqrt{3} \right) (v^2 + u^2 - 3)^2, \tag{17a}
$$

$$
\mathcal{I}_s(v, u) = -\frac{27}{4\,v^3\,u^3} (v^2 + u^2 - 3) \left[4\,v\,u + (v^2 + u^2 - 3) \log\left| \frac{3 - (v - u)^2}{3 - (v + u)^2} \right| \right], \tag{17b}
$$

where $\Theta(z)$ denotes the theta function. The function $Q^\lambda(k, p)$ arises from the polarization tensor associated with the tensor modes. It is given by

$$
Q^\lambda(k, p) = \begin{cases} \left(\frac{p}{k}\right)^2 \frac{\sin^2\theta}{\sqrt{2}}\, \cos(2\phi), & \text{for } \lambda = +, \\ \left(\frac{p}{k}\right)^2 \frac{\sin^2\theta}{\sqrt{2}}\, \sin(2\phi), & \text{for } \lambda = \times, \end{cases} \tag{18}
$$

where θ is the polar angle and ϕ is azimuthal angle associated with the wavevector $\boldsymbol{p}$ with $\boldsymbol{k}$ taken along the z-axis. The four point correlation present in Eq. (16) is the term which shall give rise to Gaussian and non-Gaussian contributions. On substituting the expression of $\mathcal{R}_{\boldsymbol{k}}$ as given in Eq. (2) in each of the four mode functions of this term, we obtain a series of terms with different powers of f_{NL}. The terms that are independent of f_{NL} are evidently the Gaussian contributions. The terms with higher powers of f_{NL} are the non-Gaussian contributions. We shall first obtain the secondary tensor power spectrum arising from the Gaussian contribution. Focusing on the terms independent of f_{NL} and using Wick's theorem, we can express the four point correlation in terms of the two point correlations. This leads to the following expression for secondary tensor power spectrum $\mathcal{P}_h(k, \eta)$ in terms of the scalar power spectrum:

$$
\mathcal{P}_h(k, \eta) = 2\, \frac{16}{81} \frac{2\,\pi^2}{k^2\,\eta^2} \int \frac{\mathrm{d}^3 \boldsymbol{k}'}{(2\pi)^3} \, Q^\lambda(k, k')\, Q_\lambda(k, k')\, \mathcal{I}^2(k, k') \, \frac{k^3\, \mathcal{P}_{\mathrm{S}}(k')\, \mathcal{P}_{\mathrm{S}}(|\boldsymbol{k} - \boldsymbol{k}'|)}{k'^3\, |\boldsymbol{k} - \boldsymbol{k}'|^3}, \tag{19}
$$

where the $\mathcal{P}_{\mathrm{s}}(k)$ denotes the Gaussian part of the scalar power spectrum. We should note that $\mathcal{P}_h(k, \eta)$ is averaged over the oscillations that occur on small time scales. Hence, the quantity $\mathcal{I}(k, k')$ can be expressed as

$$\mathcal{I}^2(k, k') = \left[\mathcal{I}_c^2\left(\frac{k'}{k}, \frac{|\boldsymbol{k} - \boldsymbol{k}'|}{k}\right) + \mathcal{I}_s^2\left(\frac{k'}{k}, \frac{|\boldsymbol{k} - \boldsymbol{k}'|}{k}\right) \right]. \tag{20}$$

Notice that the contraction of $Q(k, k')$ over λ implies summing over both polarizations. Utilizing this expression of $\mathcal{P}_h(k, \eta)$, we may express the dimensionless spectral energy density of GWs associated with secondary tensor perturbations in the current universe, *viz.* $\Omega_{\mathrm{GW}}(k)$, as [11, 36]

$$h^2 \, \Omega_{\mathrm{GW}}(k) = \frac{1.38 \times 10^{-5}}{24} \, (k^2 \, \eta^2) \, \mathcal{P}_h(k, \eta). \tag{21}$$

This corresponds to Ω_{GW} arising from the Gaussian contribution. As we further compute the non-Gaussian contributions to $\mathcal{P}_h(k)$, we shall utilize the above relation to compute the corresponding Ω_{GW} as well.

As to the non-Gaussian contributions to $\mathcal{P}_h(k)$, there shall be terms arising from the four point correlation of Eq. (16) that contain f_{NL}^2 and f_{NL}^4. Let us first consider the terms at the level of f_{NL}^2. These terms can be understood as arising when we introduce f_{NL}, as defined in Eq. (2), in two of $\mathcal{R}_{\boldsymbol{k}}$ terms of the four point correlation. This gives rise to three types of contributions to $\mathcal{P}_h(k)$, which we shall refer to as $\mathcal{P}_h^{(2-1)}(k), \mathcal{P}_h^{(2-2)}(k)$ and $\mathcal{P}_h^{(2-3)}(k)$. The exact expressions that describe these three contributions are given by

$$
\begin{aligned}
\mathcal{P}_h^{(2-1)}(k) = {} & 2^5 \, \frac{16}{81} \, \frac{9}{25} \, \frac{(2\pi^2)^2}{(2\pi)^6} \, \frac{1}{k^2 \, \eta^2} \\
& \times \int \mathrm{d}^3\boldsymbol{q}_1 \int \mathrm{d}^3\boldsymbol{q}_2 \, Q^\lambda(k, q_1) \, Q_\lambda(k, q_2) \, \mathcal{I}(k, q_1) \, \mathcal{I}(k, q_2) \\
& \times k^3 \, \frac{\mathcal{P}_{\mathrm{s}}(q_2) \, \mathcal{P}_{\mathrm{s}}(|\boldsymbol{q}_2 + \boldsymbol{k}|) \, \mathcal{P}_{\mathrm{s}}(|\boldsymbol{q}_1 - \boldsymbol{q}_2|)}{q_2^3 \, |\boldsymbol{q}_2 + \boldsymbol{k}|^3 \, |\boldsymbol{q}_1 - \boldsymbol{q}_2|^3} \\
& \times f_{\mathrm{NL}}(q_1, q_2, |\boldsymbol{q}_1 - \boldsymbol{q}_2|) \, f_{\mathrm{NL}}(|\boldsymbol{k} - \boldsymbol{q}_1|, |\boldsymbol{q}_2 - \boldsymbol{q}_1|, |\boldsymbol{k} + \boldsymbol{q}_2|),
\end{aligned} \tag{22a}
$$

$$
\begin{aligned}
\mathcal{P}_h^{(2-2)}(k) = {} & 2^5 \, \frac{16}{81} \, \frac{9}{25} \, \frac{(2\pi^2)^2}{(2\pi)^6} \, \frac{1}{k^2 \, \eta^2} \int \mathrm{d}^3\boldsymbol{q}_1 \int \mathrm{d}^3\boldsymbol{q}_2 \, Q^\lambda(k, q_1) \, Q_\lambda(k, q_1) \, \mathcal{I}^2(k, q_1) \\
& \times k^3 \, \frac{\mathcal{P}_{\mathrm{s}}(|\boldsymbol{k} - \boldsymbol{q}_1|) \, \mathcal{P}_{\mathrm{s}}(q_2) \, \mathcal{P}_{\mathrm{s}}(|\boldsymbol{q}_1 - \boldsymbol{q}_2|)}{q_2^3 \, |\boldsymbol{k} - \boldsymbol{q}_1|^3 \, |\boldsymbol{q}_1 - \boldsymbol{q}_2|^3} \, f_{\mathrm{NL}}^2(q_1, q_2, |\boldsymbol{q}_1 - \boldsymbol{q}_2|) \\
= {} & 2^5 \, \frac{16}{81} \, \frac{(2\pi^2)}{(2\pi)^3} \, \frac{1}{k^2 \, \eta^2} \\
& \times \int \mathrm{d}^3\boldsymbol{q}_1 \, Q^\lambda(k, q_1) \, Q_\lambda(k, q_1) \, \mathcal{I}^2(k, q_1) \, k^3 \, \frac{\mathcal{P}_{\mathrm{c}}(q_1) \, \mathcal{P}_{\mathrm{s}}(|\boldsymbol{k} - \boldsymbol{q}_1|)}{q_1^3 \, |\boldsymbol{k} - \boldsymbol{q}_1|^3},
\end{aligned} \tag{22b}
$$

$$
\begin{aligned}
\mathcal{P}_h^{(2-3)}(k) = {} & 2^5 \, \frac{16}{81} \, \frac{9}{25} \, \frac{(2\pi^2)^2}{(2\pi)^6} \, \frac{1}{k^2 \, \eta^2} \\
& \times \int \mathrm{d}^3\boldsymbol{q}_1 \int \mathrm{d}^3\boldsymbol{q}_2 \, Q^\lambda(k, q_1) \, Q_\lambda(k, q_2) \, \mathcal{I}(k, q_1) \mathcal{I}(k, q_2) \\
& \times k^3 \, \frac{\mathcal{P}_{\mathrm{s}}(q_1) \, \mathcal{P}_{\mathrm{s}}(q_2) \, \mathcal{P}_{\mathrm{s}}(|\boldsymbol{k} - \boldsymbol{q}_1 + \boldsymbol{q}_2|)}{q_1^3 \, q_2^3 \, |\boldsymbol{k} - \boldsymbol{q}_1 + \boldsymbol{q}_2|^3} \\
& \times f_{\mathrm{NL}}(|\boldsymbol{k} - \boldsymbol{q}_1|, q_2, |\boldsymbol{k} - \boldsymbol{q}_1 + \boldsymbol{q}_2|) \, f_{\mathrm{NL}}(|\boldsymbol{k} + \boldsymbol{q}_2|, q_1, |\boldsymbol{k}_1 - \boldsymbol{q}_1 + \boldsymbol{q}_2|).
\end{aligned} \tag{22c}
$$

We should note that the numerical factors preceding the integrals have been retained in their specific forms to give an idea of the origin of these terms. For instance, the powers of 2 arise from the various possible configurations of wavenumbers corresponding to a contribution. The fraction $9/25$ arises from the factor of $3/5$ present in the definition of f_{NL}, whereas the factors of 2π arise from the definition of power spectrum and the Fourier transformations.

Besides, we have used the definition of $\mathcal{P}_{\mathrm{c}}(k)$ in $\mathcal{P}_h^{(2-2)}(k)$ to reduce the first expression and obtain Eq. (22b) [*cf.* Eq. (14)]. Such a simplification is not possible with $\mathcal{P}_h^{(2-1)}(k)$ or $\mathcal{P}_h^{(2-3)}(k)$. It is useful to note that one can construct Feynman diagrams to represent these integrals (see, for instance, Refs. [13, 16, 17]). If we identify the diagrams with the above integrals, we find that $\mathcal{P}_h^{(2-1)}(k)$ arises from what is called the C-type diagram, whereas $\mathcal{P}_h^{(2-3)}(k)$ arises from the Z-type diagram. The term $\mathcal{P}_h^{(2-2)}(k)$ arises from what is known as the hybrid diagram (see, App. A for a discussion on these diagrams). The difference between the integrals presented here and the corresponding

ones in the literature is the dependence of f_{NL} over wavenumbers. As mentioned earlier, it has been argued that the terms $\mathcal{P}_h^{(2-1)}(k)$ and $\mathcal{P}_h^{(2-3)}(k)$ shall vanish when integrated over the azimuthal angles and it is only the $\mathcal{P}_h^{(2-2)}(k)$ term that survives [12, 14]. However, it was later shown that $\mathcal{P}_h^{(2-1)}(k)$ and $\mathcal{P}_h^{(2-3)}(k)$ do not necessarily vanish when the angular dependences are appropriately accounted for [17].

Next, we shall consider contributions to $\mathcal{P}_h(k)$ at the level of f_{NL}^4. These terms can be understood as arising from f_{NL} in all four of $\mathcal{R}_{\boldsymbol{k}}$ in the four point function in Eq. (16). In such a case, we obtain three contributions, which we shall call $\mathcal{P}_h^{(4-1)}(k), \mathcal{P}_h^{(4-2)}(k)$ and $\mathcal{P}_h^{(4-3)}(k)$. The expressions describing these contributions are given by

$$
\begin{aligned}
\mathcal{P}_h^{(4-1)}(k) = {} & 2^7\,\frac{16}{81}\left(\frac{9}{25}\right)^2\frac{(2\,\pi^2)^3}{(2\,\pi)^9}\frac{1}{k^2\,\eta^2}\int \mathrm{d}^3\boldsymbol{q}_1\int \mathrm{d}^3\boldsymbol{q}_2\,Q^\lambda(k,q_1)\,Q_\lambda(k,q_2)\\
& \times \mathcal{I}(k,q_1)\,\mathcal{I}(k,q_2)\,k^3\int \mathrm{d}^3\boldsymbol{q}_2'\,\frac{\mathcal{P}_{\mathrm{S}}(|\boldsymbol{k}-\boldsymbol{q}_1+\boldsymbol{q}_2-\boldsymbol{q}_2'|)}{|\boldsymbol{k}-\boldsymbol{q}_1+\boldsymbol{q}_2-\boldsymbol{q}_2'|^3}\\
& \times \frac{\mathcal{P}_{\mathrm{S}}(q_2')\,\mathcal{P}_{\mathrm{S}}(|\boldsymbol{q}_2-\boldsymbol{q}_2'|)\mathcal{P}_{\mathrm{S}}(|\boldsymbol{q}_1+\boldsymbol{q}_2'|)}{q_2'^{\,3}\,|\boldsymbol{q}_2-\boldsymbol{q}_2'|^3|\,\boldsymbol{q}_1+\boldsymbol{q}_2'|^3}\\
& \times f_{\mathrm{NL}}(q_1,|-\boldsymbol{q}_2'|,|\boldsymbol{q}_1+\boldsymbol{q}_2'|)\,f_{\mathrm{NL}}(|\boldsymbol{k}-\boldsymbol{q}_1|,|\boldsymbol{k}-\boldsymbol{q}_1+\boldsymbol{q}_2-\boldsymbol{q}_2'|,|\boldsymbol{q}_2'-\boldsymbol{q}_2|)\\
& \times f_{\mathrm{NL}}(q_2,q_2',|\boldsymbol{q}_2-\boldsymbol{q}_2'|)\,f_{\mathrm{NL}}(|\boldsymbol{k}+\boldsymbol{q}_2|,|\boldsymbol{q}_1-\boldsymbol{k}-\boldsymbol{q}_2+\boldsymbol{q}_2'|,|-\boldsymbol{q}_1-\boldsymbol{q}_2'|)
\end{aligned}
\tag{23a}
$$

$$
\mathcal{P}_h^{(4-2)}(k) = 2^7\,\frac{16}{81}\,\frac{(2\,\pi^2)}{(2\,\pi)^3}\,\frac{1}{k^2\,\eta^2}\int \mathrm{d}^3\boldsymbol{q}_1\,Q^\lambda(k,q_1)\,Q_\lambda(k,q_1)\,\mathcal{I}^2(k,q_1)\,k^3\,\frac{\mathcal{P}_{\mathrm{C}}(q_1)\,\mathcal{P}_{\mathrm{C}}(|\boldsymbol{k}-\boldsymbol{q}_1|)}{q_1^3\,|\boldsymbol{k}-\boldsymbol{q}_1|^3},
\tag{23b}
$$

$$
\begin{aligned}
\mathcal{P}_h^{(4-3)}(k) = {} & 2^7\,\frac{16}{81}\left(\frac{9}{25}\right)^2\frac{(2\,\pi^2)^3}{(2\,\pi)^9}\frac{1}{k^2\,\eta^2}\int \mathrm{d}^3\boldsymbol{q}_1\int \mathrm{d}^3\boldsymbol{q}_1'\,Q^\lambda(k,q_1)\,\mathcal{I}(k,q_1)\\
& \times k^3\,\frac{\mathcal{P}_{\mathrm{S}}(q_1')\,\mathcal{P}_{\mathrm{S}}(|\boldsymbol{q}_1-\boldsymbol{q}_1'|)\,\mathcal{P}_{\mathrm{S}}(|\boldsymbol{k}-\boldsymbol{q}_1+\boldsymbol{q}_1'|)}{q_1'^{\,3}\,|\boldsymbol{q}_1-\boldsymbol{q}_1'|^3\,|\boldsymbol{k}-\boldsymbol{q}_1+\boldsymbol{q}_1'|^3}\\
& \times f_{\mathrm{NL}}(q_1,q_1',|\boldsymbol{q}_1-\boldsymbol{q}_1'|)\,f_{\mathrm{NL}}(|\boldsymbol{k}-\boldsymbol{q}_1|,|-\boldsymbol{q}_1'|,|\boldsymbol{k}-\boldsymbol{q}_1+\boldsymbol{q}_1'|)\\
& \times \int \mathrm{d}^3\boldsymbol{q}_2\,Q_\lambda(k,q_2)\,\mathcal{I}(k,q_2)\,\frac{\mathcal{P}_{\mathrm{S}}(|\boldsymbol{q}_1'-\boldsymbol{q}_1-\boldsymbol{q}_2|)}{|\boldsymbol{q}_1'-\boldsymbol{q}_1-\boldsymbol{q}_2|^3}\\
& \times f_{\mathrm{NL}}(q_2,|\boldsymbol{q}_1+\boldsymbol{q}_2-\boldsymbol{q}_1'|,|\boldsymbol{q}_1'-\boldsymbol{q}_1|)\,f_{\mathrm{NL}}(|-\boldsymbol{k}-\boldsymbol{q}_2|,|\boldsymbol{q}_1'-\boldsymbol{q}_1-\boldsymbol{q}_2|,|\boldsymbol{q}_1-\boldsymbol{k}-\boldsymbol{q}_1'|).
\end{aligned}
\tag{23c}
$$

Once again, we have retained the numerical factors to understand the origin of these factors. Also, we have used the definition of $\mathcal{P}_{\mathrm{C}}(k)$ to reduce the expression of $\mathcal{P}_h^{(4-2)}(k)$ in terms of $\mathcal{P}_{\mathrm{C}}(k)$ [cf. Eq. (14)]. This is known as the reducible contribution. The other two terms, viz. $\mathcal{P}_h^{(4-1)}(k)$ and $\mathcal{P}_h^{(4-3)}(k)$, cannot be rewritten in terms of $\mathcal{P}_{\mathrm{C}}(k)$ and they correspond to so-called non-planar and planar Feynman diagrams, respectively (cf. App. A; for a discussion in this context, also see Ref. [17]).

We can now utilize Eq. (21) to compute the Ω_{GW} arising from each of these non-Gaussian contributions as well as the Gaussian contribution, and compare them against one another. However, we should note here that, the terms denoted as $\mathcal{P}_h^{(2-i)}(k)$, containing f_{NL}^2, involve computation of six dimensional integrals and the terms denoted as $\mathcal{P}_h^{(4-i)}(k)$, containing f_{NL}^4, involve performing nine dimensional integrals. Evidently, when we need to compute such integrals numerically, simpler methods such as the Boole's rule on a grid based sampling can be disadvantageous. Also, in such conventional methods, one will require enormous number of sampling points to achieve reasonable level of convergence of integrals in higher dimensions. Hence, one should resort to Monte-Carlo method of integration which circumvents the issue of dimensionality with reasonable number of points [39]. Moreover, at each point of these integrals we require the power spectra and f_{NL} to be evaluated, with their respective dependences on wavenumbers. Therefore, arriving at numerical estimates of these non-Gaussian contributions for a case of inflation driven by non-trivial potentials is a computationally intensive exercise. There has been an earlier attempt in the literature to compute these contributions [17]. But, we should point out that, in such efforts, the computations involved using analytical templates for the power spectra, such as the Dirac delta function or a lognormal function. Also, the f_{NL} was assumed to be of local form with a given amplitude and without any scale dependence. Hence, the computation of integrals in such cases is relatively easier. However, in this work we compute both the power spectra and the f_{NL} numerically from the action governing the perturbations for a given model of interest. Therefore, the computation becomes significantly more intensive and hence takes considerably more time and processing power. Due to this complexity in computation and constraints in implementation, in this work, we shall restrict ourselves to calculating the non-Gaussian contributions up to the level of f_{NL}^2, i.e. terms denoted as $\mathcal{P}_h^{(2-i)}$.

V. MODELS FOR ILLUSTRATION

In this section, we shall illustrate the calculation of the correction to the scalar power spectrum and the non-Gaussian contributions to Ω_{GW} due to a generic $f_{\mathrm{NL}}(k_1, k_2, k_3)$ using two models of inflation. These models serve as good examples of a typical scenario of inflation leading to generation of secondary GWs of significant strengths. These models permit a brief epoch of ultra slow roll leading to enhancement of scalar power over small scales. These scalar perturbations source the secondary tensor perturbations and hence amplify the strength of secondary GWs over frequencies corresponding to those scales.

The first model we shall consider is inflation driven by a potential which has a dip introduced to it by hand. Such scenarios where a bump or a dip introduced in a rather smooth potential have been discussed in the literature in the context of PBH formation [19, 20]. Though it may not be well motivated or immediately realized from a high energy theory, it is a toy model that helps achieve a brief epoch of ultra slow roll during inflation and hence enhance the scalar power. Here we shall work with such a toy model consisting of a dip added to the well known potential of Starobinsky model. The form of this potential shall be

$$V(\phi) = V_0 \left[1 - \exp\left(-\sqrt{\frac{2}{3}} \frac{\phi}{M_{\mathrm{Pl}}}\right)\right]^2 \left\{1 - \lambda \exp\left[-\frac{1}{2}\left(\frac{\phi - \phi_0}{\Delta\phi}\right)^2\right]\right\},\tag{24}$$

where clearly the first part is the potential corresponding to Starobinsky model, while the second part in curly braces is the Gaussian shaped dip located at ϕ_0 having a coupling strength λ and a width $\Delta\phi$. The values of the parameters involved are set to be $V_0 = 2.25 \times 10^{-10}\,M_{\mathrm{Pl}}^4$, $\lambda = 2.58 \times 10^{-3}$, $\phi_0 = 4.25\,M_{\mathrm{Pl}}$ and $\Delta\phi = 2.8 \times 10^{-2}\,M_{\mathrm{Pl}}$. With the initial value of $\phi_i = 5.6\,M_{\mathrm{Pl}}$, we achieve about 81 e-folds of inflation with the epoch of ultra slow roll occurring at around 50 e-folds from the beginning, as the field crosses and evolves beyond ϕ_0. We shall refer to this model as SMD, standing for Starobinsky model with a dip.

Another model we shall consider to illustrate our arguments is a model known as critical-Higgs inflation [21–23]. This model arises when the Higgs field is non-minimally coupled to gravity. The effective potential in this scenario contains a point of inflection which leads to an epoch of ultra slow roll thereby enhancing the scalar power. The potential describing this model can be written as

$$V(\phi) = V_0 \frac{\left[1 + a\,(\ln z)^2\right]\,z^4}{\left[1 + c\,(1 + b\ln z)\,z^2\right]^2},\tag{25}$$

where the quantity $z = \phi/\mu$. We shall choose the values of the parameters to be $\mu = 1\,M_{\mathrm{Pl}}$ and $V_0 = 1.5 \times 10^{-8}\,M_{\mathrm{Pl}}^4$. The other parameters involved are related to each other through the inflection point z_{c} as follows:

$$a = \frac{4}{1 + c\,z_{\mathrm{c}}^2 + 2\,\log(z_{\mathrm{c}}) - 4\,\log^2(z_{\mathrm{c}})},\tag{26a}$$

$$b = 2\,\frac{1 + c\,z_{\mathrm{c}}^2 + 4\,\log(z_{\mathrm{c}}) + 2\,c\,z_{\mathrm{c}}^2\,\log z_{\mathrm{c}}}{c\,z_{\mathrm{c}}^2\,[1 + c\,z_{\mathrm{c}}^2 + 2\,\log(z_{\mathrm{c}}) - 4\,\log^2(z_{\mathrm{c}})]}.\tag{26b}$$

We have set $\{c, z_{\mathrm{c}}\} = \{2.850, 0.784\}$ and arrived at $\{a, b\}$ using these values. For these values of the model parameters, and with an initial value of field $\phi_i = 6.0\,M_{\mathrm{Pl}}$, we achieve about 66 e-folds of inflation. The epoch of ultra slow roll occurs at around 31 e-folds from the beginning of evolution as the field crosses the inflection point at $0.784\,M_{\mathrm{Pl}}$. We shall denote this model as CHI.

The scalar power spectra arrived at from these models are presented in the left panel of Fig. 1. The power over small scales have been amplified by several orders due to the ultra slow roll epochs in these models. The parameters that we have worked with ensure that the spectra are COBE normalized over the CMB scales. However, we should mention that the predictions of n_{s} and r over these scales have some tension with the constraints on these parameters arrived at by Planck [41]. This issue is known in case of models with enhancement of power over small scales and the tension with data is larger if the peak is closer to CMB scales [10, 11]. Moreover, the rise in power occurs close to the range of scales that can be probed by the effect of spectral distortion in CMB [42–44]. Hence there is a possibility of constraining these models against data from future missions probing this effect with improved sensitivity [45]. In this work, we shall focus on the generation of secondary GWs due to the rise in power over small scales and the contributions due to scalar bispectrum.

We first compute the amplitude and behavior of secondary GWs generated from these two models due to Gaussian contribution. We present the observable quantity of interest, *viz.* the dimensionless energy density of secondary GWs, Ω_{GW} as a function of frequency f. The spectrum of $\Omega_{\mathrm{GW}}(f)$ has been plotted for our models of interest in the right panel of Fig. 1. The peak in these spectra occur at around $10^6\,\mathrm{Mpc}^{-1}$ for the choices of parameter values we have
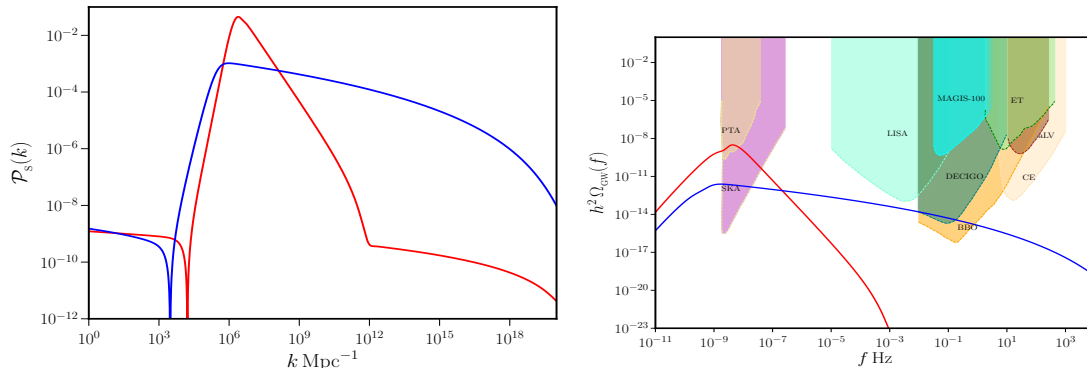
FIG. 1. The scalar power spectra (on the left) and the corresponding Ω_{GW} generated (on the right) in the models of interest are presented here (SMD in red and CHI in blue). For the values of parameters chosen for these models, we observe that the peaks of these spectra occur at around $10^6\,\mathrm{Mpc}^{-1}$. This leads to the maximum amplitudes of associated Ω_{GW} occur at around $10^{-9}\,\mathrm{Hz}$. The various constraint and sensitivity curves corresponding to current and upcoming GW missions are presented as shaded regions of different colors at the top of the plot of Ω_{GW} (on the right). The intersection of Ω_{GW} curve of CHI with the sensitivity regions of SKA and BBO indicate predictions for the corresponding future detectors. The intersection of the Ω_{GW} curve of SMD with PTA indicates the possibility of arriving at constraints on the associated model parameters by comparing with the NANOGrav data [40].

worked with. The peak produced in the case of SMD is sharper than in the model of CHI. We also plot the constraint and sensitivity curves from various current and upcoming observational missions (see Ref. [3] and the associated web-page for the sensitivity curves of various missions). We find that the maximum amplitude of the Ω_{GW} generated is over the range corresponding to PTA and SKA surveys and the curve due to SMD already intersects with the PTA constraint. This indicates possible constraining and ruling out of regions in the parameter space determining the dip in the potential using the NANOGrav data [40, 46].

Our primary objective in this work is to examine the possible imprints of the scalar non-Gaussianity on the power spectra and on the $\Omega_{\mathrm{GW}}(f)$ in these models. Hence, we begin by calculating the correction to the power spectrum by the procedure discussed earlier in section III. We first compute the scalar bispectrum for the models. We evaluate all the contributions arising from the third order action governing the scalar perturbations and arrive at the complete form of the scalar bispectra $G(k_1, k_2, k_3)$ [cf. Eqs. (8) and (9)] for each of the models. We then use the relation given in Eq. (7), to obtain the associated $f_{\mathrm{NL}}(k_1, k_2, k_3)$. This $f_{\mathrm{NL}}(k_1, k_2, k_3)$ is then substituted into Eq. (14), to finally arrive at the correction to the power spectrum $\mathcal{P}_{\mathrm{C}}(k)$. Since the bispectra for the models of interest are not easy to evaluate analytically, we perform this calculation numerically.

We present the behavior of this parameter, in Fig. 2, for both the models of interest in various limits of the configuration of wavenumbers, viz. , the squeezed limit ($\boldsymbol{k}_3 \to \boldsymbol{0}$, $\boldsymbol{k}_1 = -\boldsymbol{k}_2$), equilateral limit ($k_1 = k_2 = k_3 = k$) and the flattened limit ($k_1 = k_2 = k$, $k_3 = 2\,k$). The parameter exhibits non-trivial behavior close to the wavenumber corresponding to the peak in the power spectra. The behavior is smoother over scales farther from the peak in the spectra. We also present the density plot of f_{NL} around the peak in the power for these models in Fig 3. We find that f_{NL} is largely local in its behavior around the peak. We should note that the value of f_{NL} is lesser than unity over this range of wavenumbers close to the peak. However, we notice deviation from these local values as we move further from the peak, i.e. k_3 takes values smaller than k_1. We should mention here that there arises a sharp spike in the $f_{\mathrm{NL}}(k_1, k_2, k_3)$ at the point where there is a sharp downward spike in the power spectrum, occurring before the rise and the peak in the range of wavenumbers. This indicates power spectrum reaching very small values. Hence, quantities such as $f_{\mathrm{NL}}(k_1, k_2, k_3)$ or the scalar spectral index $n_{\mathrm{S}}(k)$ that contain power spectrum in their denominators of their definitions, may incur spuriously large values at this wavenumber. Therefore, care should be taken when dealing with such anomalous values. In our calculation, we have regulated the value of f_{NL} around the region by introducing a cutoff of 10. This implies that any value of $|f_{\mathrm{NL}}|$ which is larger than 10 is taken to be 10.

A. Calculation of the correction

With $f_{\mathrm{NL}}(k_1, k_2, k_3)$ thus computed, we can obtain the correction to the spectrum $\mathcal{P}_{\mathrm{C}}(k)$ for both the models. Before we proceed to perform the integrals numerically, we consider the Eq. (14) and attempt to arrive at a rough analytical estimate of the $\mathcal{P}_{\mathrm{C}}(k)$.
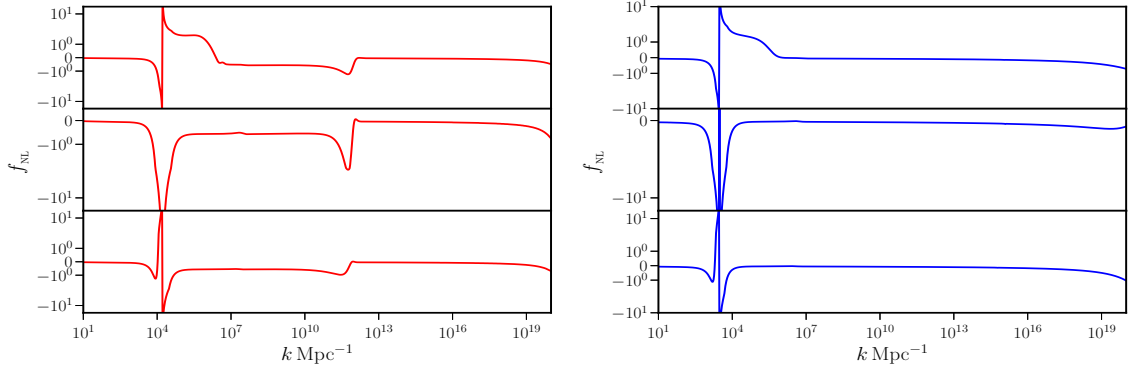
FIG. 2. We present the non-Gaussianity parameter $f_{\mathrm{NL}}(k_1, k_2, k_3)$ for the two models of interest (SMD in left and CHI in right) in various limits, *viz.* squeezed limit (on the top), equilateral limit (in the middle) and the flattened limit (in the bottom panel). We see that the $f_{\mathrm{NL}}(k_1, k_2, k_3)$ has non-trivial scale dependence and it is important to capture its complete behavior while computing the corrections to the power spectrum. There are rather large values of $f_{\mathrm{NL}}(k_1, k_2, k_3)$ occurring at the wavenumbers corresponding to the location of the sharp downward spike in the power spectra of respective models. As mentioned earlier, these spuriously large values should be dealt with caution and have to be regulated while using $f_{\mathrm{NL}}(k_1, k_2, k_3)$ in further calculations.
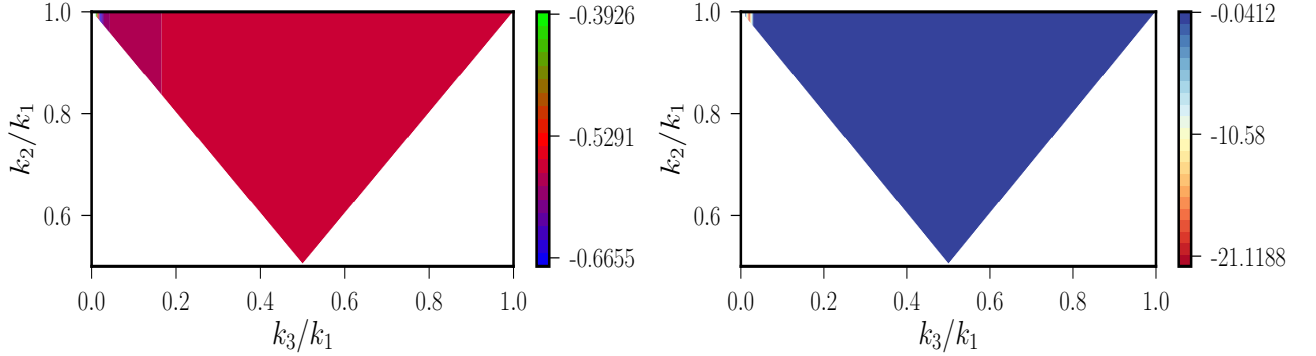
FIG. 3. The density plots of the scalar non-Gaussianity parameter $f_{\mathrm{NL}}(k_1, k_2, k_3)$ illustrating its behavior in a general configuration of wavenumbers around a given value of k_1 is presented for models of interest. The parameter obtained from SMD is plotted on the left, while the parameter from the model of CHI on the right. The behavior is evidently dependent on the value of k_1, which for both the models is taken to be $k_1 = 10^6 \, \mathrm{Mpc}^{-1}$, corresponding to the wavenumber close to the peak in the spectra. We find that the $f_{\mathrm{NL}}(k_1, k_2, k_3)$ in these models are highly local in shape just around the peak in the spectra. The value of the parameter is roughly -0.5 in case of SMD, whereas in case of CHI, it turns out to be around -0.04. As we move away from the peak, with values of $k_3 \ll k_1$, we see that the f_{NL} starts deviating from the local shape and growing larger in value.

Let k_{peak} denote the wavenumber corresponding to the peak in the power spectrum. We know that the maximum amplitude of the integrand occurs around the region where $x = k_{\mathrm{peak}}/k$ or $y = k_{\mathrm{peak}}/k$ or $x = y = k_{\mathrm{peak}}/k$. We illustrate the range of the integrals involved and the points where the maximum contribution arises from in Fig. 4. We shall describe the sharp peaking behavior of the power spectrum by approximating its form around the peak using a Dirac delta function as

$$\mathcal{P}_{\mathrm{S}}(k) = \mathcal{P}_{\mathrm{S}}(k_{\mathrm{peak}}) \, \delta(\ln(k) - \ln(k_{\mathrm{peak}})) . \tag{27}$$

Using this approximation, we proceed to compute the dominant contributions to the integrals. We perform the integral over x in Eq. (14) to obtain that

$$\mathcal{P}_{\mathrm{C}}(k) = \frac{9}{25} \left(\frac{k}{k_{\mathrm{peak}}} \right) \mathcal{P}_{\mathrm{S}}(k_{\mathrm{peak}}) \int_{|1 - k_{\mathrm{peak}}/k|}^{1 + k_{\mathrm{peak}}/k} \frac{\mathrm{d}y}{y^2} \mathcal{P}_{\mathrm{S}}(ky) \, f_{\mathrm{NL}}^2(k, k_{\mathrm{peak}}, ky) \tag{28}$$

Now we shall consider the two regimes in wavenumbers, *viz.* $k < k_{\mathrm{peak}}$ and $k > k_{\mathrm{peak}}$. For the case of $k < k_{\mathrm{peak}}$, the integrand receives contribution only from the point P3 marked in Fig. 4. Due to the narrow range of the integral over
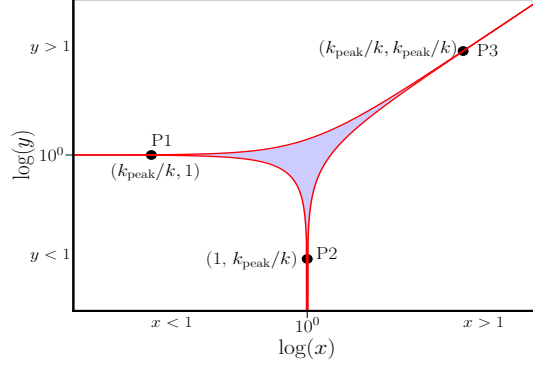
FIG. 4. The range of integration involved in calculating $\mathcal{P}_{\mathrm{C}}(k)$ [*cf.* Eq. (14)] is plotted in logarithmic scale. The shaded region marks the region covered by the limits of the integrals. We mark the three points P1, P2 and P3 at which the integrals derive maximum contribution when there is a localized peak in the power spectrum. The region around the points P1 and P2 contribute for $k > k_{\mathrm{peak}}$ and the region around P3 contributes for $k < k_{\mathrm{peak}}$. It is also worth noting that, due to the symmetry of the integrand over the variables x and y the contributions from P1 and P2 turn out to be equal to one another. For the case of $k \sim k_{\mathrm{peak}}$ the integrand receives the maximum contribution from the wide region around $x = y = 1$.

y, we may approximate $ky \simeq k_{\mathrm{peak}}$ in the arguments of $\mathcal{P}_{\mathrm{S}}$ and f_{NL}. So, the above integral over y simplifies to

$$\mathcal{P}_{\mathrm{C}}(k) \simeq \frac{9}{25}\left(\frac{k}{k_{\mathrm{peak}}}\right)\left[\mathcal{P}_{\mathrm{S}}(k_{\mathrm{peak}})f_{\mathrm{NL}}(k,k_{\mathrm{peak}},k_{\mathrm{peak}})\right]^2 \int_{|1-k_{\mathrm{peak}}/k|}^{1+k_{\mathrm{peak}}/k} \frac{\mathrm{d}y}{y^2}$$
$$= \frac{18}{25}\left(\frac{k}{k_{\mathrm{peak}}}\right)^3 \left[\mathcal{P}_{\mathrm{S}}(k_{\mathrm{peak}})f_{\mathrm{NL}}(k,k_{\mathrm{peak}},k_{\mathrm{peak}})\right]^2 , \tag{29}$$

where we have used the fact that $k_{\mathrm{peak}}/k > 1$. It is interesting to note the combination of wavenumbers appearing in the argument of f_{NL}. We know that $k < k_{\mathrm{peak}}$. Hence, $f_{\mathrm{NL}}(k,k_{\mathrm{peak}},k_{\mathrm{peak}})$ denotes that the parameter has to be evaluated in the squeezed limit of the configuration of wavenumbers. This further simplifies the expression because we know that the consistency condition relating the f_{NL} and the scalar spectral index $n_{\mathrm{s}}(k)$ is obeyed in these models [11, 18]. Therefore, we utilize the consistency relation *i.e.*

$$f_{\mathrm{NL}}(k,k_{\mathrm{peak}},k_{\mathrm{peak}}) = \frac{5}{12}\left[n_{\mathrm{s}}(k_{\mathrm{peak}}) - 1\right]. \tag{30}$$

Here, strictly speaking, $[n_{\mathrm{s}}(k_{\mathrm{peak}}) - 1]$ vanishes identically since it is the slope of the spectrum at its peak. However, we shall take it to be a small non-vanishing value close to the peak in the spectrum for the purpose of our calculation. Therefore expression for $\mathcal{P}_{\mathrm{C}}(k)$ reduces to

$$\mathcal{P}_{\mathrm{C}}(k) = \frac{1}{8}\left(\frac{k}{k_{\mathrm{peak}}}\right)^3 \left\{\mathcal{P}_{\mathrm{S}}(k_{\mathrm{peak}})\left[n_{\mathrm{s}}(k_{\mathrm{peak}}) - 1\right]\right\}^2 . \tag{31}$$

We find that $\mathcal{P}_{\mathrm{C}}(k)$ shall be proportional to k^3 over the scales with $k < k_{\mathrm{peak}}$.

We then consider the case of $k > k_{\mathrm{peak}}$. For these wavenumbers, there arise contributions from two points, P1 and P2 as marked in Fig. 4. We shall first evaluate the contribution at P1 using the approximation of the spectrum in Eq. (27). The expression for $\mathcal{P}_{\mathrm{C}}(k)$ becomes

$$\mathcal{P}_{\mathrm{C}}(k) \simeq \frac{9}{25}\left(\frac{k}{k_{\mathrm{peak}}}\right)\mathcal{P}_{\mathrm{S}}(k_{\mathrm{peak}})\mathcal{P}_{\mathrm{S}}(k)f_{\mathrm{NL}}^2(k,k_{\mathrm{peak}},k) \int_{|1-k_{\mathrm{peak}}/k|}^{1+k_{\mathrm{peak}}/k} \frac{\mathrm{d}y}{y^2}$$
$$= \frac{18}{25}\mathcal{P}_{\mathrm{S}}(k_{\mathrm{peak}})\mathcal{P}_{\mathrm{S}}(k)f_{\mathrm{NL}}^2(k,k,k_{\mathrm{peak}}) , \tag{32}$$

where we have used the smallness of k_{peak}/k. We again note that the arguments of f_{NL} suggest that it is evaluated in the squeezed limit but now with k_{peak} acting as the squeezed mode. Hence we shall make use of the consistency relation again, where

$$f_{\mathrm{NL}}(k,k,k_{\mathrm{peak}}) = \frac{5}{12}\left[n_{\mathrm{s}}(k) - 1\right]. \tag{33}$$

This reduces the expression for $\mathcal{P}_{\mathrm{C}}(k)$ to

$$\mathcal{P}_{\mathrm{C}}(k) = \frac{1}{8}\mathcal{P}_{\mathrm{S}}(k_{\mathrm{peak}})\mathcal{P}_{\mathrm{S}}(k)\left[n_{\mathrm{S}}(k)-1\right]^2 . \tag{34}$$

Due to the fact that the form of the integral in Eq. (14) remains unchanged under the exchange of x and y, the contribution from the point P2 shall be the same as given above. So, we have the total value of $\mathcal{P}_{\mathrm{C}}(k)$ for $k > k_{\mathrm{peak}}$ to be

$$\mathcal{P}_{\mathrm{C}}(k) = \frac{1}{4}\mathcal{P}_{\mathrm{S}}(k_{\mathrm{peak}})\mathcal{P}_{\mathrm{S}}(k)\left[n_{\mathrm{S}}(k)-1\right]^2 . \tag{35}$$

We find that $\mathcal{P}_{\mathrm{C}}(k)$ over this regime of $k > k_{\mathrm{peak}}$ shall be proportional to $\mathcal{P}_{\mathrm{S}}(k)$ with no explicit scale dependence. If the spectrum turns nearly scale invariant away from the peak over large wavenumbers, then we can expect a corresponding $\mathcal{P}_{\mathrm{C}}(k)$ with nearly constant amplitude. In summary, we have the analytical estimate of $\mathcal{P}_{\mathrm{C}}(k)$ to be

$$\mathcal{P}_{\mathrm{C}}(k) = \begin{cases} \dfrac{1}{8}\left(\dfrac{k}{k_{\mathrm{peak}}}\right)^3 \{\mathcal{P}_{\mathrm{S}}(k_{\mathrm{peak}})[n_{\mathrm{S}}(k_{\mathrm{peak}})-1]\}^2 , & \text{for } k < k_{\mathrm{peak}} , \\ \dfrac{1}{4}\,\mathcal{P}_{\mathrm{S}}(k_{\mathrm{peak}})\mathcal{P}_{\mathrm{S}}(k)\left[n_{\mathrm{S}}(k)-1\right]^2 , & \text{for } k > k_{\mathrm{peak}} . \end{cases} \tag{36}$$

Having obtained these analytical expressions, we proceed to compute the exact numerical estimates of $\mathcal{P}_{\mathrm{C}}(k)$. We shall briefly discuss certain aspects of numerical evaluation of the integrals involved. The integral is evaluated ensuring that the regime of $x = k_{\mathrm{peak}}/k$ and $y = k_{\mathrm{peak}}/k$ are well sampled. Due to the wide range of the integral over x, the integration is performed over log scale. The limits are chosen such that the range of integration is centered at k_{peak}/k and spans two decades on either side of the point. For given values of kx and ky, the power spectra is evaluated numerically. Besides, each point of this x–y plane provides a triangular configuration of wavenumbers for which $f_{\mathrm{NL}}(k, kx, ky)$ is evaluated numerically. This is the most time consuming part of the calculation. Once computed, the integrand is summed over to obtain $\mathcal{P}_{\mathrm{C}}(k)$. The exercise is repeated for complete range of wavenumbers.

B. Calculation of non-Gaussian contributions to Ω_{GW}

The behavior of $\mathcal{P}_{\mathrm{C}}(k)$ may give us an idea of the effect of f_{NL} on the scalar power spectrum. It may further give us an insight about the amplitude of one of the non-Gaussian contributions to Ω_{GW} [cf. Eqs. (22)]. Having obtained the $\mathcal{P}_{\mathrm{C}}(k)$ in the models of interest, we proceed to compute the non-Gaussian contributions $\mathcal{P}_h^{(2-i)}$ to the Ω_{GW} in these cases.

At the outset, we should note that, the non-trivial dependence of f_{NL} over different combination of wavenumbers in $\mathcal{P}_h^{(2-1)}(k)$, $\mathcal{P}_h^{(2-2)}$ and $\mathcal{P}_h^{(2-3)}(k)$ do not allow us to easily obtain an analytical estimate as we did for $\mathcal{P}_{\mathrm{C}}(k)$. Hence, as mentioned earlier, we numerically perform these integrals involved using the Monte-Carlo method of integration. Let us now mention a few details about the procedure. We first identify the region of maximum amplitude of the integrands in the range of integration, for a given wavenumber k. Interestingly, we find that the integrands have maximum values around the wavenumber k_{peak}, if the wavenumber of interest $k < k_{\mathrm{peak}}$, while they peak around k if $k > k_{\mathrm{peak}}$. We also find that the nature of integrands are very localized in the range of k allowing us to set the range of integrals to be two decades on either side of the peaks of the integrands. The respective angular integrals are performed over the entire range viz. $\cos\theta_i \in [-1, 1]$ and $\phi_i \in [0, 2\pi]$. During the performance of integration, each point corresponds to numerical evaluation of a combination of power and bi-spectra with their appropriate arguments of wavenumbers. The computation of f_{NL} at each point of integration is the time consuming part of this process. The integrals were performed using 10^5 points and checked for convergence.

We should also note an interesting property of these contributions. The integrand describing $\mathcal{P}_h^{(2-2)}(k)$ is positive definite and hence the contribution shall be positive. However, the integrand characterizing the contributions $\mathcal{P}_h^{(2-1)}(k)$ and $\mathcal{P}_h^{(2-3)}(k)$ can be negative, because of their dependence over the polar angles (as noted earlier in Ref. [17]). This property should be accounted for while comparing them against Ω_{GW} obtained from the Gaussian contribution.

C. Results

First, we present the $\mathcal{P}_{\mathrm{C}}(k)$, obtained both the analytically and numerically, against the original spectra, $\mathcal{P}_{\mathrm{S}}(k)$, in Fig. 5. We observe that $\mathcal{P}_{\mathrm{C}}(k)$ is smaller than the original $\mathcal{P}_{\mathrm{S}}(k)$ particularly around the peak and over the range
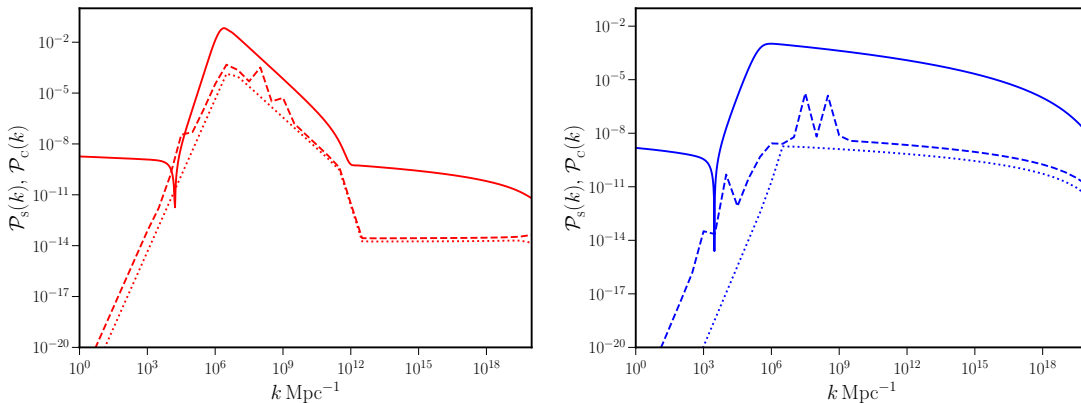
FIG. 5. The original scalar power spectra $\mathcal{P}_{\mathrm{S}}(k)$ (as solid lines) and the non-Gaussian corrections $\mathcal{P}_{\mathrm{C}}(k)$ due to the bispectrum (as dashed lines) have been plotted here for the models of interest, *viz.* SMD (on the left) and CHI (on the right). Evidently, the $\mathcal{P}_{\mathrm{C}}(k)$ computed is lower in amplitude than $\mathcal{P}_{\mathrm{S}}(k)$. We have also plotted the analytical estimate of $\mathcal{P}_{\mathrm{C}}(k)$ for these two models (as dotted lines). The analytical estimate matches the numerical behavior better in the case of SMD than CHI since the spectrum is more sharply peaked in the first model than in the second model. The complete spectrum corrected for $\mathcal{P}_{\mathrm{C}}(k)$ shall effectively be the same as the original $\mathcal{P}_{\mathrm{S}}(k)$, particularly around k_{peak} and over $k > k_{\mathrm{peak}}$.

$k > k_{\mathrm{peak}}$. There appears a region close to the dip in the spectrum where $\mathcal{P}_{\mathrm{C}}(k)$ is greater than $\mathcal{P}_{\mathrm{S}}(k)$. This is mainly due to the sharp spike occurring in f_{NL} that we mentioned earlier. But apart from this effect, there arises no significant correction to the original power spectrum. Moreover, the analytical estimate fairly mimics the exact numerical behavior of $\mathcal{P}_{\mathrm{C}}(k)$. The behavior of k^3 over large scales and near scale invariance over small scales is well captured in the numerical result thereby assuring the validity of the analytical estimates over wavenumbers far from the peak. The match is better for the model SMD. This can be understood because its spectrum is closer in resemblance to the Dirac delta function used in the analytical calculation. The original spectrum $\mathcal{P}_{\mathrm{S}}(k)$ in case of CHI has a rather broad peak with slower descent over the range of wavenumbers. This behavior leads to the difference between numerical and analytical estimates of $\mathcal{P}_{\mathrm{C}}(k)$ around the peak in this model. However, for $k > k_{\mathrm{peak}}$, the analytical estimate matches better even in case of such a broad peak. The rugged nature of the numerical result is due to the limited number of points taken for evaluation over the range of wavenumbers.

We present the behavior of the non-Gaussian contributions to Ω_{GW} at the level of f_{NL}^2, *viz.* due to $\mathcal{P}_h^{(2-i)}(k)$, in Fig. 6. We focus particularly around the peak amplitude of Ω_{GW} and find that the non-Gaussian contributions are significant for SMD. These contributions dominate the Ω_{GW} from the Gaussian spectrum for wavenumbers $k \leq k_{\mathrm{peak}}$. However, they become sub-dominant for $k > k_{\mathrm{peak}}$. In case of CHI, the non-Gaussian contributions become briefly comparable over the range of $k \simeq k_{\mathrm{peak}}$. But they are sub-dominant for wavenumbers $k < k_{\mathrm{peak}}$ as well as $k > k_{\mathrm{peak}}$. Thus, we learn that the behavior of Ω_{GW} arising from non-Gaussian contributions are highly model dependent and significant in case of power spectrum with highly localized behavior around the peak. However, as we move farther from the peak, these contributions become lesser in amplitude compared to the Gaussian contribution. Therefore, these models illustrate that the non-Gaussian contributions to Ω_{GW} have to be computed and consistently accounted for, especially around the peak of the spectral density.

VI.   CONCLUSION

There have been attempts in the literature to account for scalar non-Gaussianity in the calculation of the spectral density of the secondary GWs, $\Omega_{\mathrm{GW}}(f)$, for specific cases of f_{NL} assuming certain shapes or limits of the bispectrum. In this work, we have presented a method to account for a general scalar bispectrum with non-trivial scale dependence in such a calculation. We have presented the correction to the scalar power spectrum that may arise due to the scalar bispectrum. We have also attempted an analytical estimate of the correction to be expected from models with a localized peak in the power spectrum. We have found that it is the squeezed limit of f_{NL} that contributes the most to the correction for wavenumbers away from the peak in the power spectrum. We have then presented the non-Gaussian contributions to $\Omega_{\mathrm{GW}}(f)$ that arise due to f_{NL}. We have computed terms that are reducible in terms of $\mathcal{P}_{\mathrm{C}}(k)$ as well as those that are not reducible so. We have consistently accounted for the scale dependence of f_{NL}, arising from the modified definition of the parameter, in computing these contributions.

We then illustrated our method using two models of inflation. These are models driven by canonical scalar fields
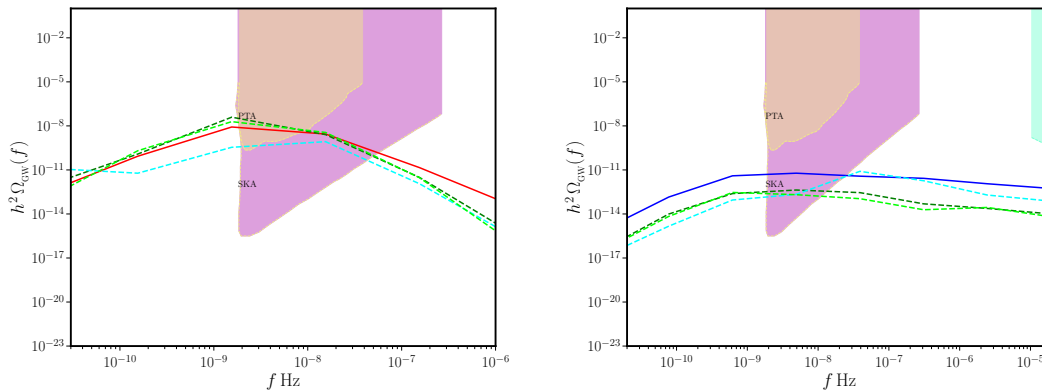
FIG. 6. We present the non-Gaussian contributions to $\Omega_{\rm GW}$ arising due to $f_{\rm NL}$ (as dashed lines), against the original Gaussian contribution (as solid lines) for the models SMD (on left) and CHI (on right), focusing over the range of frequencies containing the maximum amplitude. The contributions arising from the terms $\mathcal{P}_h^{(2-1)}(k)$ (in green), $\mathcal{P}_h^{(2-2)}(k)$ (in cyan), $\mathcal{P}_h^{(2-3)}(k)$ (in lime) are presented for both the models of interest.

that permit brief epochs of ultra slow roll and hence lead to significant amplitudes of secondary GWs. We have computed the correction to the power spectrum arising from $f_{\rm NL}$ and find that it is largely sub-dominant to the original power spectrum. Moreover, the analytical estimate of the correction agrees fairly well with the exact numerical estimate in these cases. We have then computed the non-Gaussian contributions to the $\Omega_{\rm GW}(f)$ and compared them against the Gaussian contribution. We have computed these contributions up to the level of $f_{\rm NL}^2$. We have found that the non-Gaussian contributions are non-trivial and slightly different from the shape of the original $\Omega_{\rm GW}(f)$. The non-Gaussian contributions arising in the case of SMD have been found to dominate the original amplitudes of $\Omega_{\rm GW}(f)$ around the frequencies corresponding to the wavenumber $k_{\rm peak}$ containing the peak in the power spectrum, as well as smaller wavenumbers, *i.e.* over $k < k_{\rm peak}$. But, these contributions decrease farther from the peak and become sub-dominant to the Gaussian contribution for wavenumbers with $k > k_{\rm peak}$. In the case of CHI, the non-Gaussian contribution become briefly comparable to and dominant over the Gaussian contribution around $k_{\rm peak}$, but remain sub-dominant farther from $k_{\rm peak}$ on either side. Since the models serve as examples typical models of inflation that are considered in this context of generation of secondary GWs, we can argue that the non-Gaussian contributions arising from $f_{\rm NL}$ may turn out to be significant, particularly around the peak amplitude of $\Omega_{\rm GW}$. Hence, they have to be computed and accounted for in the estimates of $\Omega_{\rm GW}$.

Besides, we should emphasize that the method used for calculation has its value in being able to capture the complete behavior of $f_{\rm NL}(k_1, k_2, k_3)$ in any non-trivial scenario of inflation. Moreover, the analytical estimate of the correction to the power spectrum, $\mathcal{P}_{\rm C}(k)$, serves as a good approximation for the exact estimate, without directly computing the bispectrum. This greatly reduces the time taken for the calculation of $f_{\rm NL}$ and provides a quick estimate of $\mathcal{P}_{\rm C}(k)$ to be expected from just the shape of the spectrum for any model with a peak in its scalar power. Importantly, the non-negligible levels of non-Gaussian contributions to $\Omega_{\rm GW}$ obtained in these models indicate the necessity to capture the exact scale dependence of $f_{\rm NL}$ as presented in this method.

As to the caveats of this work, we should mention that we have restricted the computation of non-Gaussian contributions to $\Omega_{\rm GW}$ up to terms involving $f_{\rm NL}^2$ due to the complexity of numerical implementation. We are currently working on addressing the complexity and accounting for terms involving $f_{\rm NL}^4$ in the calculation. Secondly, there arises a spike like behavior in the shape of $f_{\rm NL}$ [*cf.* Fig. 2]. This occurs due to the presence of $\mathcal{P}_{\rm S}(k)$ in the denominator of the expression of $f_{\rm NL}$ in terms of power and bi-spectra [*cf.* Eq. (7)]. As $\mathcal{P}_{\rm S}(k)$ reaches extremely small values, this spike occurs and it has to be regulated to a finite value during the computation. This has an effect in our results as one may see a corrugated shape of $\mathcal{P}_{\rm C}(k)$ computed using $f_{\rm NL}$. Hence, to avoid such artefacts in computation, it may be preferable to modify this method to utilize the bispectrum directly in the calculation of $\mathcal{P}_{\rm C}(k)$ as well as the non-Gaussian contributions to $\Omega_{\rm GW}$. We are presently working on these issues.

In summary, we argue that the method we have discussed is a robust way to account for the exact form of primordial scalar non-Gaussianity at the level of three point correlation in the calculation of $\Omega_{\rm GW}$ arising from models of inflation. Since we infer a significant non-Gaussian contribution to $\Omega_{\rm GW}$ in the models considered, it would be interesting to employ this method for non-canonical models that can potentially produce larger amplitudes and different shapes of scalar non-Gaussianities. Such scenarios may even lead to significant non-Gaussian corrections to the power spectra along with large non-Gaussian contributions to $\Omega_{\rm GW}$. Moreover there are efforts to account for the contribution of higher

order non-Gaussianities, such as the trispectrum, to the secondary tensor power spectrum. It would be interesting to explore the effects of non-Gaussianities with non-trivial scale dependence in such higher order calculations.

ACKNOWLEDGMENTS

Appendix A: Feynman diagrams for non-Gaussian contributions to Ω_{GW}

In order to understand various non-Gaussian contributions to the secondary GWs, one can construct Feynman diagrams representing these contributions (see, for instance, Refs. [13, 16, 17]). In this appendix, we shall define the elements constituting these diagrams and present the diagrams corresponding to the contributions we discussed in Sec. IV.

The basic elements that we shall be using for the diagrams are the scalar power spectrum $\mathcal{P}_{\mathrm{S}}(k)$, secondary tensor power spectrum $\mathcal{P}_h(k)$, the scalar non-Gaussianity parameter $f_{\mathrm{NL}}(k_1, k_2, k_2)$ and the correction to the scalar power spectrum $\mathcal{P}_{\mathrm{C}}(k)$. These diagrams are presented in Fig. 7. Note that the diagram representing the secondary tensor power spectrum $\mathcal{P}_h(k)$ indicates that it is a one loop correction to the primary tensor power spectrum, due to the interaction between the tensor and scalar perturbations at the second order. The functions $\mathcal{I}(k, k')$ and $Q^\lambda(k, k')$ arising out of the transfer function and polarization tensor, can be accounted at the vertices connecting the secondary tensor and scalar modes in the diagram of $\mathcal{P}_h(k)$. The diagram of $f_{\mathrm{NL}}(k_1, k_2, k_2)$ represents the interaction of scalar perturbations $\mathcal{R}_{\boldsymbol{k}}$ at the cubic order. Further, the diagram of $\mathcal{P}_{\mathrm{C}}(k)$ indicates that it is a one loop correction to the
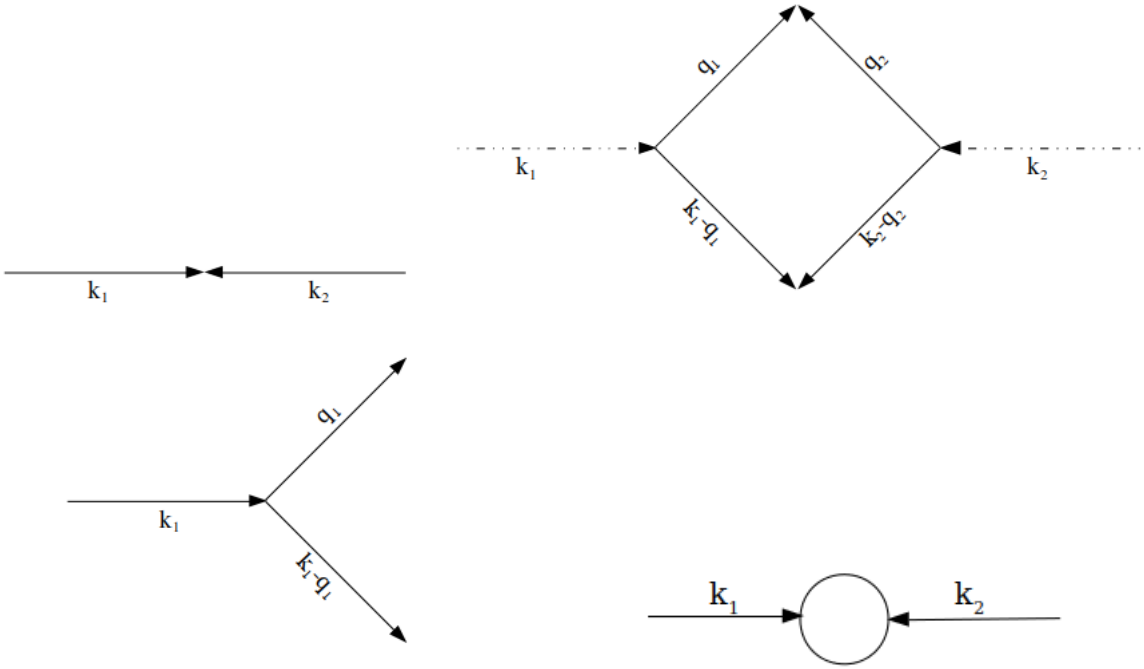

FIG. 7. The Feynman diagrams representing the scalar power spectrum $\mathcal{P}_{\mathrm{S}}(k_1)$ (on top left), secondary tensor power spectrum $\mathcal{P}_h(k_1)$ (on top right) are presented. We also present the diagrams for the scalar non-Gaussianity parameter $f_{\mathrm{NL}}(k_1, q_1, |\boldsymbol{k}_1 - \boldsymbol{q}_1|)$ (on bottom left) and the correction to the scalar power $\mathcal{P}_{\mathrm{C}}(k_1)$ (on bottom right). We use solid lines to represent the scalar mode $\mathcal{R}_{\boldsymbol{k}}$ and dashed-dotted line to represent the secondary tensor mode $h_{\boldsymbol{k}}$.
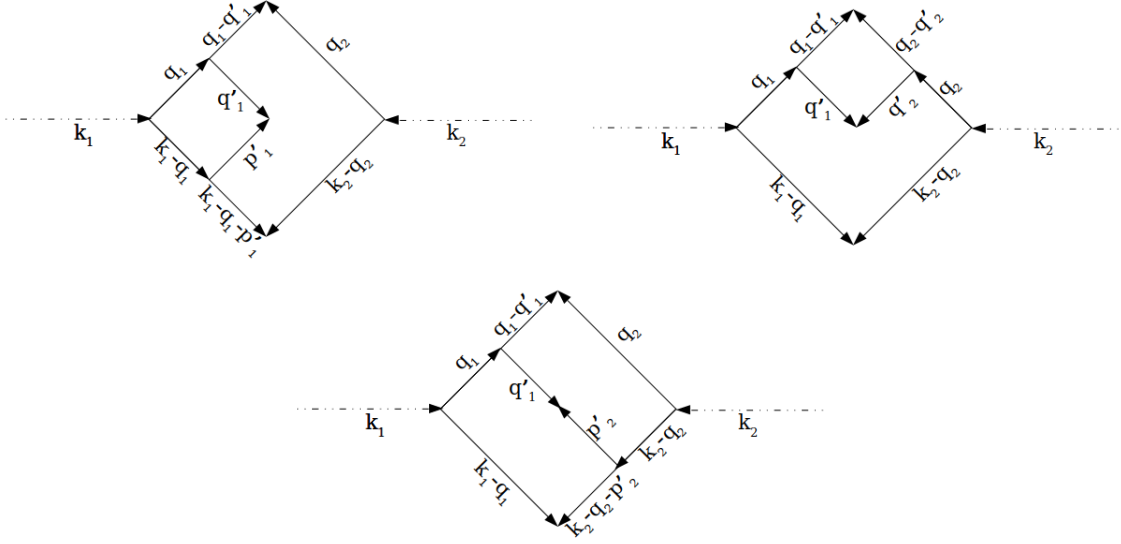
FIG. 8. The Feynman diagrams representing the non-Gaussian contributions at the level of $f_{\rm NL}^2$ are presented. The term denoted as $\mathcal{P}_h^{(2-1)}(k)$ corresponds to the C-type diagram (on top left) and the term denoted as $\mathcal{P}_h^{(2-2)}(k)$ corresponds to the diagram known as the hybrid type (on top right). The term denoted as $\mathcal{P}_h^{(2-3)}(k)$ corresponds to the Z-type diagram (at the bottom).
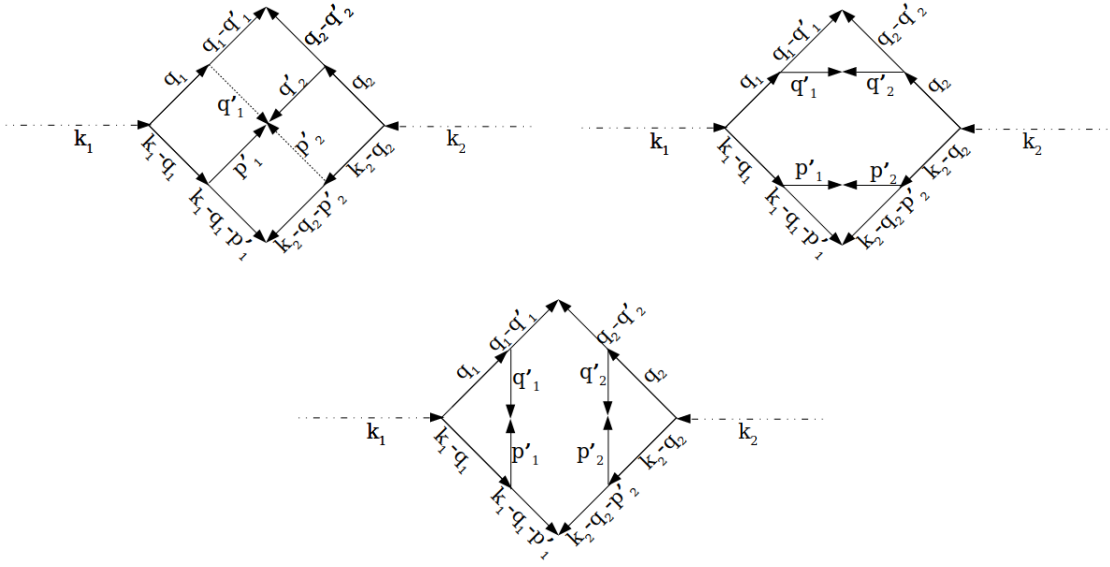

FIG. 9. The Feynman diagrams representing the non-Gaussian contributions at the level of $f_{\rm NL}^4$ are presented. The term denoted as $\mathcal{P}_h^{(4-1)}(k)$ corresponds to non-planar diagram (on top left). Note that the dotted arrows are scalar modes that meet outside the plane of the diagram. The term denoted as $\mathcal{P}_h^{(4-2)}(k)$ corresponds to the diagram known as reducible term (on top right). The term denoted as $\mathcal{P}_h^{(4-3)}(k)$ corresponds to the planar diagram (at the bottom).

scalar power spectrum $\mathcal{P}_{\rm S}(k)$ due to such cubic order interaction. It involves two vertices of $f_{\rm NL}$ and hence we readily infer that $\mathcal{P}_{\rm C}(k)$ shall be proportional to $f_{\rm NL}^2$. Using these elements we can construct the diagrams for higher order contributions to secondary tensor power spectrum $\mathcal{P}_h(k)$ due to scalar non-Gaussianity. These shall be higher order loop diagrams arising due to introduction of the vertex of $f_{\rm NL}$ in each arm of the loop in the diagram of $\mathcal{P}_h(k)$.

The diagrams representing non-Gaussian contributions to $\mathcal{P}_h(k)$ at the level of $f_{\rm NL}^2$, $\mathcal{P}_h^{(2-i)}(k)$, are presented in Fig. 8. These diagrams arise due to the introduction of $f_{\rm NL}$ in two of the four arms of the loop in the diagram of $\mathcal{P}_h(k)$. They are called as C-type, hybrid and Z-type diagrams [17].

The diagrams representing non-Gaussian contributions to $\mathcal{P}_h(k)$ at the level of f_{NL}^4 *i.e.* $\mathcal{P}_h^{(4-i)}(k)$, are presented in Fig. 9. These diagrams arise when we introduce of f_{NL} in all the four arms of the loop in the diagram of $\mathcal{P}_h(k)$. They are called as non-planar, reducible and planar diagrams [17].

[1] K. N. Ananda, C. Clarkson, and D. Wands, Phys. Rev. **D75**, 123518 (2007), arXiv:gr-qc/0612013 [gr-qc].
[2] D. Baumann, P. J. Steinhardt, K. Takahashi, and K. Ichiki, Phys. Rev. **D76**, 084019 (2007), arXiv:hep-th/0703290 [hep-th].
[3] C. Moore, R. Cole, and C. Berry, Class. Quant. Grav. **32**, 015014 (2015), arXiv:1408.0740 [gr-qc].
[4] J. Garcia-Bellido, M. Peloso, and C. Unal, JCAP **1709** (09), 013, arXiv:1707.02441 [astro-ph.CO].
[5] N. Bartolo, V. De Luca, G. Franciolini, M. Peloso, D. Racco, and A. Riotto, Phys. Rev. D **99**, 103521 (2019), arXiv:1810.12224 [astro-ph.CO].
[6] B. Carr, K. Kohri, Y. Sendouda, and J. Yokoyama, (2020), arXiv:2002.12778 [astro-ph.CO].
[7] J. Garcia-Bellido and E. Ruiz Morales, Phys. Dark Univ. **18**, 47 (2017), arXiv:1702.03901 [astro-ph.CO].
[8] C. Germani and T. Prokopec, Phys. Dark Univ. **18**, 6 (2017), arXiv:1706.04226 [astro-ph.CO].
[9] I. Dalianis, A. Kehagias, and G. Tringas, JCAP **01**, 037, arXiv:1805.09483 [astro-ph.CO].
[10] N. Bhaumik and R. K. Jain 10.1088/1475-7516/2020/01/037 (2019), [JCAP2001,037(2020)], arXiv:1907.04125 [astro-ph.CO].
[11] H. V. Ragavendra, P. Saha, L. Sriramkumar, and J. Silk, Phys. Rev. D **103**, 083510 (2021), arXiv:2008.12202 [astro-ph.CO].
[12] R.-g. Cai, S. Pi, and M. Sasaki, Phys. Rev. Lett. **122**, 201101 (2019), arXiv:1810.11000 [astro-ph.CO].
[13] C. Unal, Phys. Rev. D **99**, 041301 (2019), arXiv:1811.09151 [astro-ph.CO].
[14] R.-G. Cai, S. Pi, S.-J. Wang, and X.-Y. Yang, JCAP **05**, 013, arXiv:1901.10152 [astro-ph.CO].
[15] H. V. Ragavendra, L. Sriramkumar, and J. Silk, JCAP **05**, 010, arXiv:2011.09938 [astro-ph.CO].
[16] V. Atal and G. Domènech, JCAP **06**, 001, arXiv:2103.01056 [astro-ph.CO].
[17] P. Adshead, K. D. Lozanov, and Z. J. Weiner, (2021), arXiv:2105.01659 [astro-ph.CO].
[18] F. Zhang, J. Lin, and Y. Lu, (2021), arXiv:2106.10792 [gr-qc].
[19] V. Atal, J. Garriga, and A. Marcos-Caballero, JCAP **09**, 073, arXiv:1905.13202 [astro-ph.CO].
[20] S. S. Mishra and V. Sahni, JCAP **04**, 007, arXiv:1911.00057 [gr-qc].
[21] J. M. Ezquiaga, J. Garcia-Bellido, and E. Ruiz Morales, Phys. Lett. **B776**, 345 (2018), arXiv:1705.04861 [astro-ph.CO].
[22] F. Bezrukov, M. Pauly, and J. Rubio, JCAP **02**, 040, arXiv:1706.05007 [hep-ph].
[23] M. Drees and Y. Xu, Eur. Phys. J. C **81**, 182 (2021), arXiv:1905.13581 [hep-ph].
[24] J. M. Maldacena, JHEP **05**, 013, arXiv:astro-ph/0210603.
[25] J. Martin and L. Sriramkumar, JCAP **01**, 008, arXiv:1109.5838 [astro-ph.CO].
[26] F. Schmidt and M. Kamionkowski, Phys. Rev. D **82**, 103002 (2010), arXiv:1008.0638 [astro-ph.CO].
[27] I. Agullo, D. Kranas, and V. Sreenath, Front. Astron. Space Sci. **8**, 703845 (2021), arXiv:2105.12993 [gr-qc].
[28] D. K. Hazra, L. Sriramkumar, and J. Martin, JCAP **05**, 026, arXiv:1201.0926 [astro-ph.CO].
[29] V. Sreenath, D. K. Hazra, and L. Sriramkumar, JCAP **02**, 029, arXiv:1410.0252 [astro-ph.CO].
[30] H. V. Ragavendra, D. Chowdhury, and L. Sriramkumar, (2020), arXiv:2003.01099 [astro-ph.CO].
[31] D. Seery and J. E. Lidsey, JCAP **06**, 003, arXiv:astro-ph/0503692.
[32] X. Chen, Adv. Astron. **2010**, 638979 (2010), arXiv:1002.1416 [astro-ph.CO].
[33] H. Collins, (2011), arXiv:1101.1308 [astro-ph.CO].
[34] F. Arroja and T. Tanaka, JCAP **05**, 005, arXiv:1103.1102 [astro-ph.CO].
[35] K. Inomata, M. Kawasaki, K. Mukaida, Y. Tada, and T. T. Yanagida, Phys. Rev. **D95**, 123510 (2017), arXiv:1611.06130 [astro-ph.CO].
[36] J. R. Espinosa, D. Racco, and A. Riotto, JCAP **1809**, 012, arXiv:1804.07732 [hep-ph].
[37] K. Kohri and T. Terada, Phys. Rev. D **97**, 123532 (2018), arXiv:1804.08577 [gr-qc].
[38] S. Pi and M. Sasaki, (2020), arXiv:2005.12306 [gr-qc].
[39] W. H. Press, S. A. Teukolsky, W. T. Vetterling, and B. P. Flannery, *Numerical Recipes: The Art of Scientific Computing*, 3rd ed. (Cambridge University Press, Cambridge, England, 2007).
[40] Z. Arzoumanian *et al.* (NANOGrav), Astrophys. J. Lett. **905**, L34 (2020), arXiv:2009.04496 [astro-ph.HE].
[41] Y. Akrami *et al.* (Planck), (2018), arXiv:1807.06211 [astro-ph.CO].
[42] J. Chluba, A. L. Erickcek, and I. Ben-Dayan, Astrophys. J. **758**, 76 (2012), arXiv:1203.2681 [astro-ph.CO].
[43] D. Jeong, J. Pradler, J. Chluba, and M. Kamionkowski, Phys. Rev. Lett. **113**, 061301 (2014), arXiv:1403.3697 [astro-ph.CO].
[44] T. Kite, A. Ravenni, S. P. Patil, and J. Chluba, Mon. Not. Roy. Astron. Soc. **505**, 4396 (2021), arXiv:2010.00040 [astro-ph.CO].
[45] J. Chluba *et al.*, (2019), arXiv:1909.01593 [astro-ph.CO].
[46] Z. Arzoumanian *et al.* (NANOGRAV), Astrophys. J. **859**, 47 (2018), arXiv:1801.02617 [astro-ph.HE].